# RETRIVAL OF ATMOSPH ERIC AEROSOL OPTICAL AND MICROPHYSICAL PARAMETERS FROM GROUND BASE PASSIVE REMOTE SENSING MEASUREMENT OVER ADDIS ABABA

**By**

**Melaku Tesfaye**

**SUBMITTED IN PARTIAL FULFILLMENT OF THE**

**REQUIREMENTS FOR THE DEGREE OF**

**MASTER OF SCIENCE IN PHYSICS**

**AT**

**ADDIS ABABA UNIVERSITY**

**ADDIS ABABA ETHIOPIA**

**MARCH 2009**

**ADDIS ABABA UNIVERSITY**

**DEPARTMENT OF**

**PHYSICS**

The undersigned hereby certify that they have read and recommend to the Faculty of Graduate Studies for acceptance a thesis entitled "RETRIVAL OF ATMOSPHERIC AEROSOL OPTICAL AND MICROPHYSICAL PARAMETERS FROM GROUND BASE PASSIVE REMOTE SENSING MEASUREMENT OVER ADDIS ABABA." by Melaku Tesfaye in partial fulfillment of the requirements for the degree of Master of Science in physics.

Dated: March 2009

**External Examiner:**

**Dr. Feleke zewge**

**Research Advisor:**

**Dr. Gizaw Mengistu**

# ADDIS ABABA UNIVERSITY

Dated: **March 2009**

Author: **Melaku Tesfaye**

Title: **RETRIVAL OF ATMOSPH ERIC AEROSOL OPTICAL AND MICROPHYSICAL PARAMETERS FROM GROUND BASE PASSIVE REMOTE SENSING MEASUREMENT OVER ADDIS ABABA**

Department: **Physics**

Degree: **M.Sc.** Convocation: **March** Year: **2009**

Permission is herewith granted to Addis Ababa University to circulate and to have copied for non-commercial purposes, at its discretion, the above title upon the request of individuals or institutions.

Signature of Author

# Table of Contents

# Acknowledgements

I wish to express my warmest and profound gratitude first to my advisor, Dr.Gizaw Mengistu, for his positive and constructive guidance, advice, comments, and useful suggestions throughout this thesis. I would like to acknowledge gratefully Mr. Tesfaye Mamo and Mr. Tasew shared their ideas, technical advice and assistance with their relevant discussions during the constriction of homemade pyrheliometer at AAU.

I am grateful to all my friends, Bezayew G/Michale, Temesgen Yerdaw, Tamerat Nega, Semahegn Abayneh and all those whose names could not be mentioned. Their help and cooperation made the implementation this thesis possible.

March 2009 Melaku Tesfaye

# Abstract

Aerosol optical depth is determined from measurements of atmospheric effective spectral transmission, for clear-sky days on May 21, 2008 and May 23, 2008, at Addis Ababa (9° 1′ 48″ N, 38° 44′ 24″ E) carried out using pyrheliometer, which we constructed in department of physics at AAU. It has effective discrete optical channels in the range between 0.699 $\mu m$ and 0.753 $\mu m$. With in framework of Mie theory and non-linear inversion method, column integrated effective optical and microphysical parameters are retrieved. The effective refractive index, temporal variation related to atmospheric particle size distribution, and modeling the effect of water vapor implies that, atmospheric aerosols have chemically distinct compositions due to their different sources and the hygroscopic growth is facilitated by chemical alterations. Removal processes of particles are more efficient when the aerosol size increases. Retrieved real part of effective refractive index ranges between 1.53 and 1.59 while computed single scattering albedo ($\omega_0$) ranges between 0.98 and 0.99. This is indicating that dust is by far the dominant aerosol component in Addis Ababa.

# Introduction

Earth's atmosphere is composed primarily of nitrogen and oxygen with much lesser amounts of minor gases such as carbon dioxide, argon and water vapor, and small solid and liquid particles suspended in the air, called aerosols. Some aerosols are naturally produced from volcanoes, sea spray, sand, or wind-driven erosion of surface soil. Some aerosols are a result of human activity, such as dust from agricultural activities, smoke from burning biomass and fossil fuels and photo chemically induced smog due primarily to vehicle emissions [1].

Most aerosols are in the troposphere, but large volcanic eruptions can inject aerosols and trace gases much higher into the stratosphere. Aerosols in the stratosphere may remain for years while in the troposphere, precipitation and interactions with Earth's surface depends on their size, chemistry and height in the atmosphere remove aerosols in times range from minutes to days.

Aerosol concentrations vary significantly with location and time. There are seasonal and diurnal variations as well as unpredictable changes due to events such as large dust storms and volcanic eruptions. Aerosols are highly mobile; they can cross-oceans and mountain ranges. It is generally agreed that, because of higher concentrations of aerosols, skies in many parts of the world are hazier than they were one or two centuries ago, even in rural areas [2].

Each of these atmosphere components interacts with solar (or shortwave) and terrestrial (thermal or long wave) radiation in different ways. Gas molecules having a very small size (0.1 nm) compared to the wavelength of the solar radiation ($0.3\,\mu m$ to ~$5\ \mu m$) or the terrestrial radiation (greater than $5\,\mu m$) predominantly scatter solar radiation by a process known as Rayleigh scattering at the same frequency, thus producing secondary radiation which has well defined angular characteristics. Rayleigh scattered light intensity depends on the $4^{th}$ power of the light frequency (reciprocal of the wavelength) with the result that blue light is scattered about 10 times more strongly than red light (thus giving rise to blue color of the sky). In addition, gases absorb light in discrete frequencies throughout the solar spectrum, and more so in the thermal infrared (especially near the surface where their densities are high) giving rise to the well-known greenhouse effect. Increase in concentration of these molecules throughout the atmosphere, as is observed in the case of carbon dioxide and other trace gases due to human activities such as fossil

fuel burning, enhances the greenhouse warming near the surface and thus provides a source of net heating of the surface and lower atmosphere (positive forcing).

Aerosol particles are much larger than molecules; they range in radius (for spherical particles) from a few nanometers (an aggregate of tens of molecules), a result of the process of nucleation, to tens of micrometers, as in the case of sea-salt and desert dust. Cloud particles are typically larger, up to hundreds of micrometers (even larger for rain clouds) a result of condensation of water vapor on the surfaces of aerosols in an atmosphere that is super-saturated. Because the wavelength of light is now of the same order as the characteristic size of the particles (aerosols) or are less than the size of cloud particles, the light interaction with the particles is much more complex and is much stronger (per particle) for both scattering (for spherical particles this is known as Mie scattering) and absorption. Typically in an urban atmosphere the number concentration of aerosol particles tends to be high, with the result that the scattering by particles is of the same order (or higher) as that of the more numerous molecules [3].

It is well known that aerosols can have a variety of important impacts on the environment. Aerosols affect the Earth's energy budget by scattering and absorbing radiation (direct effect) and by modifying the cloud amount, lifetime, and microphysical and radiative properties (indirect effects). Moreover, the direct absorption of radiant energy by aerosols leads to heating of the troposphere and cooling of the surface, which can change the relative humidity and atmospheric stability thereby influencing the clouds and precipitation (semi-direct effect). In addition, aerosols, also known as particulate matter, have long been recognized as pollutants of concern and may have detrimental effects on human health, such as impairment of pulmonary function.

However, the quantitative assessment of the contribution of aerosols to radiative processes and monitoring of atmospheric aerosol are uncertain because of, first compared to atmospheric gases; aerosol is highly inhomogeneous and variable. That is, incomplete knowledge of aerosol macro-physical properties (sources, sinks, and loading) and of aerosol microphysical properties (composition, size distribution, chemical interaction, lifetime, and diurnal variation). Second, the available accuracy of aerosol characterization is often not sufficient. Thus quantification of their influences and to track events that alter dynamical processes of atmospheric aerosols measurements of aerosol microphysical properties are required.

Remote sensing methods are one of the main measurement techniques, for atmospheric aerosol optical and microphysical parameters. The basic principle associated with remote sensing of the atmospheric aerosols involves the interpretation of radiometric measurements of electromagnetic radiation in specific spectral intervals, which are sensitive to some physical aspects of the medium: the interaction of electromagnetic radiation with matter modifies to some extent the incident wave. The medium therefore produces a signature in the amplitude, phase or spectral composition, which depends on composition and structure of the medium.

The interaction of aerosols with radiation depends primarily on the aerosol radius ($r$) and the wavelength ($\lambda$) of radiation. The largest interaction occurs when the aerosol size parameter $x = \frac{2\pi r}{\lambda} \approx 5$. Consequently, the longer-lived accumulation mode interacts with the shortwave solar radiation spectrum to a greater extent than with the long wave infrared spectrum emitted by the Earth's atmosphere and surface, which peaks at $\lambda$ ~ $7\,\mu m$. Optical properties of aerosols may be described using a number of parameters. Scattered and absorbed radiation from an incident beam is defined by the total scattering ($\sigma_s$) and absorption coefficients ($\sigma_a$) respectively, which are a measure of the fractional change in beam intensity per meter. Radiation scattered into the backward hemisphere is correspondingly described by the hemispheric backscattering coefficient ($\sigma_{back\ scat.}$). The sum of $\sigma_s$ and $\sigma_a$ is the extinction coefficient $\sigma_{ext}$ ($\sigma_s + \sigma_a = \sigma_{ext}$) and when integrated over the beam path length *dl* gives the aerosol optical depth (AOD) $\tau$ ($\tau = \int \sigma_{ext} dl$) (AOD implicitly refers to aerosol extinction optical depth $\tau_{ext}$, the sum of aerosol absorption optical depth $\tau_a$ and aerosol scattering optical depth $\tau_s$).

An important parameter in global aerosol models is the ratio of scattering to extinction, otherwise known as the single scattering albedo $\omega_0$: $\omega_0 = \frac{\sigma_s}{\sigma_{ext}}$. The sensitivity of the particle extinction efficiency to wavelength i.e., $\left|\frac{\partial Q_{ext}(\lambda, r)}{\partial \lambda}\right|$, generally increases with decreasing particle size. This sensitivity holds true for any particle composition, and may be easily demonstrated using Mie codes. An empirical measure of this sensitivity is obtained by defining the Ångström exponent or Ångström parameter $\alpha$:

$$\alpha = \frac{\ln\left[\frac{\tau_{ext}(\lambda_1)}{\tau_{ext}(\lambda_2)}\right]}{\ln\left[\frac{\lambda_1}{\lambda_2}\right]}.$$

Typical values of $\alpha$ range from ~ 4 for gases, ~ 2 for urban pollution (sulfate) and for small carbonaceous aerosols (smoke), and ~ 1–2 for rural haze, and ~ 0 for coarse aerosols (for large dust particles). Hence if $\alpha$ can be measured then information on the number size distribution is gained and vice versa. The asymmetry factor $g$ is defined as the cosine-weighted mean of the angular scattering phase function $P(\theta)$, where $P(\theta)$ describes the amount of light scattered through an angle $\theta$:

$$g = \langle \cos\theta \rangle = \frac{\int P(\theta)\cos\theta \, d(\cos\theta)}{\int P(\theta) d(\cos\theta)}.$$

The value of $g$ ranges from -1 for complete back scattering to +1 for complete forward scattering. The asymmetry factor is important in radiative models of the atmosphere and takes the angular scattering of radiation into account. As direct measurement is not possible, it may be parameterized by the hemispheric backscattering ratio $\frac{\sigma_{back\ scat.}}{\sigma_s}$.

Aerosol optical thickness (AOT, also called aerosol optical depth) is a measure of the extent to which aerosols affect the passage of sunlight through the atmosphere. The larger the optical thickness at a particular wavelength, the less light of that wavelength reaches Earth's surface. Measurements of aerosol optical thickness at more than one wavelength can provide important information about the concentration, size distribution, and variability of aerosols in the atmosphere. This information is needed for climate studies, for comparison with remote sensing data and to understand the local and global distribution and variability of aerosols. Also taken together with other atmospheric measurements, help to better understand dynamical processes of atmospheric aerosols and predict climate. There may be observable relationships between aerosols and temperature, cloud cover, relative humidity, and precipitation.

Following the above verities, the main intentions of this thesis work are using ground-based passive remote sensing technique to quantify key microphysical and optical parameters of aerosol over Addis Ababa. Associated with those retrieved and compute column-mean optical and microphysical parameters to provide measurement-based significant speculative information's about dynamic process of atmospheric aerosols and modification processes.

The thesis is organized as follows: In chapter one, we present, the earth atmospheric aerosol with their important impacts and physico-chemical properties briefly. At the end, we introduce ground-based remote sensing techniques for atmospheric aerosol optical and microphysical parameter measurement. In chapter two, we present, Mie scattering, electromagnetic wave equation and its solution, and the far field solutions and extinction parameters.

In chapter three, we present theory of direct- solar spectral irradiance measurement and retrieval of microphysical properties of aerosols from direct- solar spectral irradiance measurements. In chapter four, we present, homemade pyrheliometer and passive solar tracker (PST) specifications with the proposed analysis. In chapter five, we present the results, discussions, validation and conclusions.

# Chapter 1: Atmospheric aerosol

In this chapter, we review briefly some general information about the earth atmospheric aerosols, important aerosol types that occur in the earth atmosphere, radiative and climatic impacts of aerosols, and physico-chemical properties of aerosols. At the end, we introduce ground-based remote sensing techniques for atmospheric aerosol optical and microphysical parameter measurement.

## 1.1 Atmospheric Aerosols

### 1.1.1 What are atmospheric Aerosols?

Atmospheric aerosols usually means the mixture of solid and liquid particles, which referred to those solid and liquid particles suspended in the atmosphere. This excludes the solid and liquid water particles in clouds, fog and rain. This definition of atmospheric aerosols encompasses a broad array of different substances with widely varying shapes, sizes, sources, sinks, and physical and chemical properties. The size of aerosol particles ranges from diameters range over four orders of magnitude (sizes from ~ 3 nanometers, nm, to a few hundredths of millimeters, mm, generally smaller than cloud droplets). The number density typically ranges from a few hundred to more than $10^6$ particles per $cm^3$ [4].

Atmospheric aerosols are originated from direct man's activities; these anthropogenic aerosols are often observable as dust, smoke, haze, and in and downwind of urban environments, as smog [5]. Others originate from natural processes, such as, wind generated dust and sea spray, volcanic eruption, smokes from natural forest fire and so on. They are directly injected to the atmosphere as coarse mode particles or primary particles (size greater than $1\,\mu m$). The natural chemical reaction of precursor natural gases is other means for production of aerosols from natural processes. These are known as secondary particles. The secondary particles are also mainly divided into two: the nucleation mode particles (size less than $0.1\,\mu m$), formed from gas to particles conversion mechanisms and the accumulation mode particles (size between $0.1\,\mu m$ and $1\,\mu m$), formed mostly by the coagulation of two or more nucleation particles [4].

| Natural | Anthropogenic |
|---|---|
| **Primary** | **Primary** |
| Mineral aerosol | Industrial dust |
| Sea salt | Soot |
| volcanic dust | Biomass burning |
| Organic aerosols | |
| **Secondary** | **Secondary** |
| Sulfates from biogenic gases | Sulfates from $SO_2$ |
| Sulfates from volcanic $SO_2$ | Organic aerosols from $VOC_s$ |
| Organic aerosols from $VOC_s$ | Nitrates from $NO_x$ |
| Nitrates from $NO_x$ | |

Note: VOC = Volatile Organic Compound

Table 1.1 Summary of the main sources of aerosols

### 1.1.2 Important aerosol types that occur in the Earth atmosphere

Condensation aerosols originate mainly from natural and anthropogenic emissions of $SO_2$, $H_2S$, $NO_x$, and carbonaceous components. Sulfate and nitrate aerosols are mainly formed by homogeneous condensation of sulfuric and nitric acid $H_2SO_4$ and $HNO_3$, i.e. the oxidation products of these emissions. Sulfate and nitrate aerosols are also primarily responsible for acid deposition. Primary particles have radii on the order of 10 nm and grow by coagulation with other aerosol particles. The particle radii usually do not exceed $1\,\mu m$ [6, 7].

Dispersion aerosols are mainly sea spray, mineral soil particles raised by the wind, volcanic debris, and mineral and organic particles raised by forest and bush fires. These particles are much larger than particles formed by condensation from the gas phase and have linear dimensions ranging from about $0.1\,\mu m$ up to $100\,\mu m$.

Sea salt particles originate from ocean water droplets. These droplets are emitted from collapsing bubbles that are formed in breaking waves. The released droplets partially dry out and leave behind salt droplets with high salt concentrations or salt particles with radii in the sub micrometer regime. This process is efficient when the near surface wind speed

exceeds 3m/s. Wet deposition is a very efficient removal process due to the hygroscopy of sea salt particles[8].

Mineral dust aerosol originates mainly from dry deserts [9]. In terms of mass, mineral dust aerosol has the largest source strength of all aerosol types. The sources of soil-derived aerosol are located on the continents, mainly at low latitudes. Here, the pronounced vertical mixing can transport the particles many kilometers high. The largest part of the tropospheric mineral aerosol is usually present in the lowest 5 km. The source strength depends critically on the wind speed and the turbulent state of the boundary layer as well as on local soil properties, topography, hydrology etc. [10].

Soil particles can be detached from the ground when the shear force of the air exceeds the adhesion force that ties the particles to the surface. Particles that fall back on the ground may pass on some of their impulse to other soil particles and detach them from the ground. If the wind speed exceeds about 0.5m/s avalanche, effects can be triggered and many particles are released into the boundary layer. This process is size selective, since adhesion forces between particle and the ground are important for particles with radii lower than a few tenth of a micrometer. Another size selection results from the fact that particles require a certain mass in order to cross the laminar layer of air and thus enter the turbulent regime where efficient vertical transport is possible. Consequently, most of the mass is released in the size range from $1\,\mu m$ to $10\,\mu m$ [7].

Mineral dust is removed from the atmosphere by gravitational settling followed by dry deposition and is scavenged by seeding cloud condensation and colliding with falling raindrops and snow [11]. Dry deposition preferentially removes dust with sizes larger than $7\,\mu m$ [12]. The long lifetime of stratospheric mineral aerosols is related to the low humidity and the absence of efficient wet deposition processes.

During volcanic eruptions, large quantities of ash can be released into the atmosphere. The volcanic debris is small irregular particles and may have a spongy structure. The linear dimensions are between $0.1\,\mu m$ and $100\,\mu m$. During the strong eruptions of the volcanoes, a large amount of volcanic ash was thrown into the stratosphere. The global aerosol load was doubled compared to the ’clean’ atmosphere before the outbreak [12].

### 1.1.3 Implications for weather and climate

Aerosols in the atmosphere have direct and indirect effects on the Earth's climate. The direct effect is related to their optical properties. Indeed, aerosols act to scatter and/or absorb solar and terrestrial radiation. The level of scattering and absorption depends on their physical and chemical characteristics. Consequently, aerosols act to modify the Earth's radiation budget and thus influence the warming/cooling of the planet. For example, non-absorbing aerosols (sulfates and sea-salt) reflect sunlight back into space providing cooling of the atmosphere and when the aerosol particles are highly absorbing, aerosols (black carbonaceous (soot) particles) have a relatively high absorption coefficient. In such a case, the sign of the forcing attributable to aerosols tends to be the same as in the case of absorbing gases.

In addition, indirectly by acting as cloud condensation nuclei (that is by serving as the particles on which cloud droplets form and grow) and, thereby, affecting cloud microphysical, radiative properties and precipitation processes [13]. The greater the number concentration of aerosol particles, the greater the number concentration of cloud drops, and hence the greater the probability of scattering of incident radiation, and hence the brighter the cloud; this effect is commonly referred to as the first aerosol indirect effect, or the Twomey effect. Likewise, the greater the number concentration of cloud drops, the less efficient the formation of precipitation, and hence the greater the persistence of the cloud, and hence the greater the time-average reflectance of solar radiation; this effect is commonly referred to as the second aerosol indirect effect, or Albrecht effect. Moreover, the direct absorption of radiant energy by aerosols can influence the atmospheric temperature structure, that is, leads to heating of the troposphere and cooling of the surface. Which can change the relative humidity, cloud droplet evaporation rate and atmospheric stability– a phenomenon that has been labeled the “semi-direct effect” [14]. All the above influences of the atmospheric aerosols are summarized in Fig. 1.2.

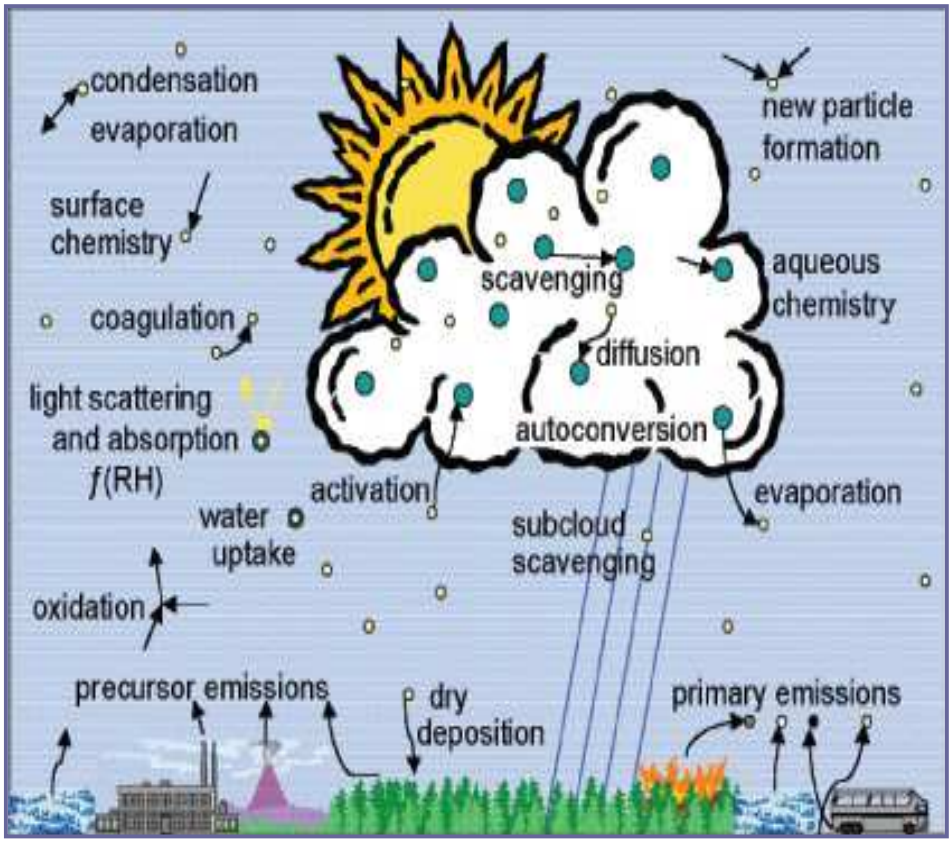


Figure 1.1: Major aerosol processes that influence climate (adapted from [15]).

## 1.1.4 Physico-chemical properties of aerosols

Much of the difficulty in quantifying aerosol influences arises from the heterogeneity of aerosol loading and properties: spatial, temporal, size, and composition. This multidimensional heterogeneity makes the characterization of aerosols and quantification of their influences on climate and climate change extremely challenging. The aerosol direct and indirect effect strongly depends on the physico-chemical properties of aerosols.

**(a) Chemical composition**

Compared to atmospheric gases, chemical composition of aerosols are complex and extremely variable in space and time; nevertheless, typical compositions can be determined. This is due to widely varying aerosol primary sources, secondary aerosol production and evolution in the atmosphere and atmospheric processes depending on the

geographical region, transportation and transformation mechanisms. These and other properties of aerosols make their chemical composition characterization extremely difficult. Size is normally used to classify aerosol because it is the most easily measured property and because inferences about the other properties can be drawn from size information [16].

Although numerous trace elements are found in the chemical compositions of aerosols, major atmospheric aerosol originate from anthropogenic activities and natural processes with their predominant composition and size ranges (modes) information (Fine particles: accumulation and nucleation mode- size ranges < 1μm and Coarse particles- size ranges >1μm) are summarized in table 1.2

| **Natural** | | | **Anthropogenic** | | |
|---|---|---|---|---|---|
| **Primary** | **Size** | **Composition** | **Primary** | **Size** | **Composition** |
| Soil Dust | >1μm | Si, Al, Fe, Ca, | Industrial Particulate | >1μm | Si, Al, Fe, heavy metals |
| Sea salt | >1μm | Na, Cl, S | Dust | >1μm | C, N, Si, Al, Fe, Ca,.. |
| Volcanic dust | >1μm | Si, Al, Fe | Soot | <1μm | C |
| Biological Debris | >1μm | C | Biomass burning | <1μm | S |
| **Secondary** | **Size** | **Composition** | **Secondary** | **Size** | **Composition** |
| Sulfates from biogenic gases | <1μm | S | Sulfates from $SO_2$ | <1μm | C, K, metals |
| Sulfates from volcanic $SO_2$ | <1μm | S | Man-made $VOC_s$ | <1μm | N |
| Organics from biogenic $VOC_s$ | <1μm | C | Nitrates from $NO_x$ | <1μm | C, N |
| Nitrates from $NO_x$ | >1μm | Na | Organics from anthropogenic $VOC_s$ | <1μm | C |

Table 1.2: Major types of atmospheric aerosol originate from both natural and human processes, predominant compositions and their corresponding size ranges (adapted from [17]).

NOTE: The distinction between fine and coarse particles is a fundamental because, in general, the fine and coarse particles mode originate and transformed separately, also removed from the atmosphere by different mechanisms, have different chemical composition, have different optical properties, etc. Thus, knowing of the major types of aerosol composition in relation to their size ranges (modes) can be used as an interpretive framework to study their origins and fates in the atmosphere.

Usually, rural aerosols are assumed to be composed of ammonium sulfate ($(NH_4)_2SO_4$) and insoluble mineral material [16].

The urban aerosol is assumed to be composed of 80% rural aerosols and 20% soot. Mineral acids like sulfuric acid or nitric acid produced mainly from gaseous precursors due to emissions from stationary (industry) and mobile (ground transportation) combustion sources. These are observed in higher concentrations in urban environments. Aerosols in coastal urban regions may contain some sea salt. Soluble organic and inorganic material is major components of aerosols in the troposphere [17].

Small maritime aerosols are assumed to be 100% ammonium sulfate (gas-to-particle conversion of $SO_2$), while large particles are pure NaCl (sea spray evaporation). In addition, maritime aerosols are composed of soluble inorganic salts such as magnesium chloride, nitrates or other organic material. Detailed description of aerosol chemical composition is given by [18].

**(b) Size distribution**

Aerosol size distributions describe the number of particles observed to have a certain radius, for various size ranges. Model size distributions have been constructed by fitting lognormal functions to data representing typical aerosol concentration for urban, rural and maritime environments (Fig.1.3). It is observed that urban environments are characterized by higher concentrations of aerosol particles (as much as $10^5$ particles per $cm^3$), while the maritime environment is characterized by the lowest particle concentrations (maximum of 100 particles per $cm^3$).

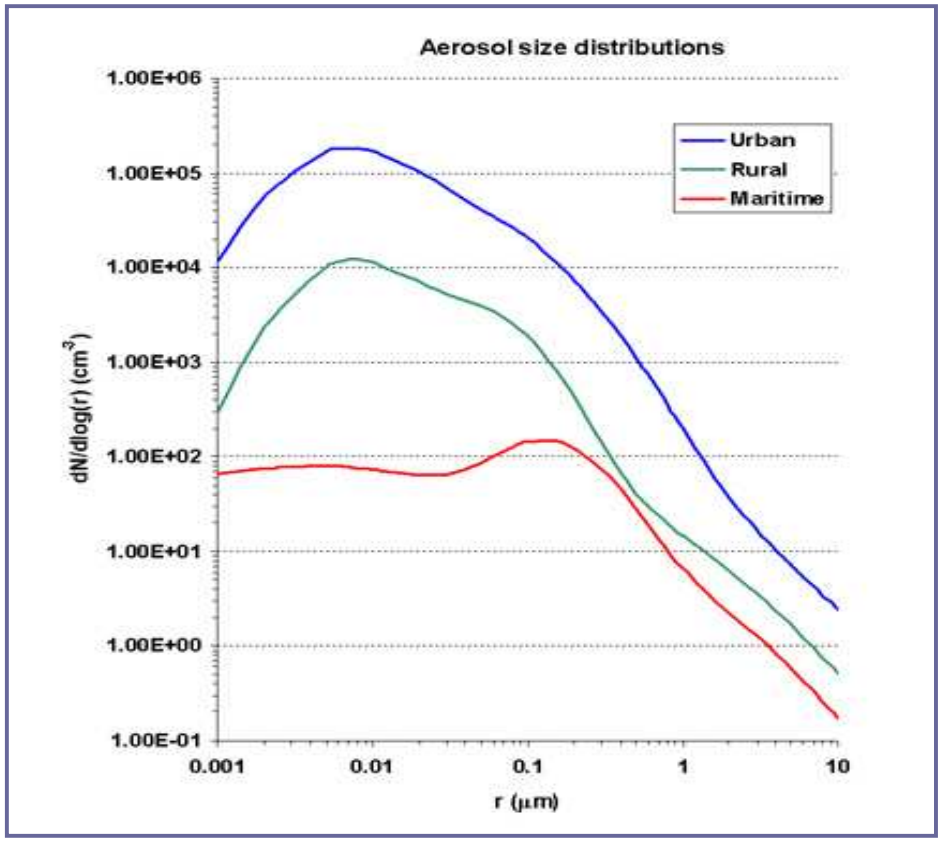


Figure 1.2: Model size distributions describing the aerosol concentrations for urban, rural and maritime environments (taken from [19]).

**(c) Radiative properties**

Aerosols particles play an important role in radiative budget of the atmosphere. The scattering and absorption of radiation by a single aerosol particle is expressed by its complex refractive index ($m = m_r + im_i$), where the real part represents scattering and the imaginary part represents absorption. The refractive index is strongly dependent on the chemical composition of the particle. Non-absorbing aerosols increase the reflection of sunlight by the atmosphere. This leads to a net cooling effect (negative values of radiative forcing). Strongly absorbing aerosols such as black carbon heat the troposphere (positive radiative forcing).

Following [17], the real and imaginary parts of the complex refractive index for urban, rural and maritime aerosols, as a function of wavelength, are shown in Fig.1.4. The results for pure water are shown as references.

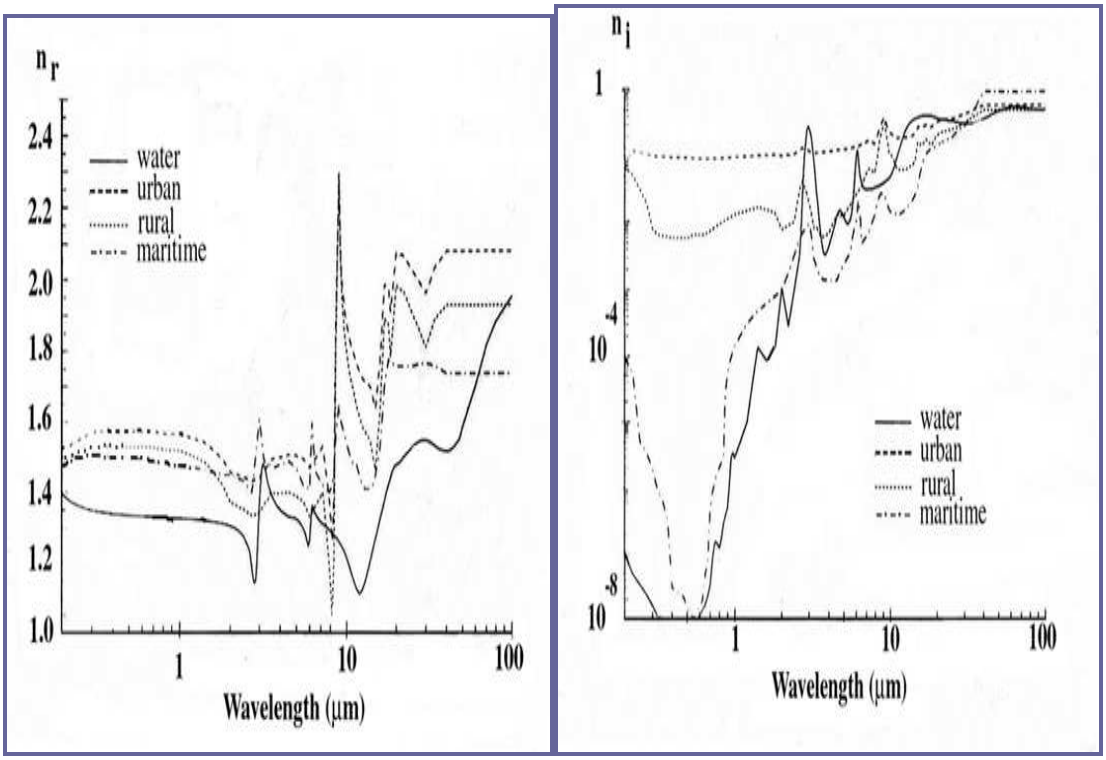


(a) (b)

Figure 1.3: Real (a), and imaginary (b), parts of the complex refractive index for different aerosol models (taken from [19]).

## 1.2 Ground-based remote sensing

In the broadest sense, remote sensing is the small or large-scale acquisition of information of an object or phenomenon, by the use of either recording or real-time sensing device(s) that is not in physical or intimate contact with the object. Remote sensing makes it possible to collect data on dangerous or inaccessible areas. Remote sensing of the atmosphere classified broadly into two categories, namely passive remote sensing and active remote sensing methods.

In passive remote sensing methods, the source is beyond the control of the observer. Passive sensors detect natural energy (radiation) that is emitted or reflected by the object or surrounding area being observed. Reflected sunlight is the most common source of radiation measured by passive sensors. Examples of passive remote sensors include radiometer, photometer, spectrometer, etc.

In active remote sensing methods, the source can be controlled by the observer. Active instruments, emits energy in order to scan objects and areas whereupon a passive sensor then detects and measures the radiation that is reflected or backscattered from the target. One of the main examples of active remote sensing instrument is LIDAR (LIght Detection And Ranging).

Among the several means of remote sensing method to measure the aerosols parameters, we highlight the ground-based remote sensing, in particular the sun photometric technique.

Sun-photometer is a ground-based passive remote sensing instrument used for measurements of the spectral transmission of solar radiation through the atmosphere using rather simple and relatively inexpensive instruments pointed directly at the sun. Pyrheliometer is the simplest sun-photometer. From the measurement one can determine Aerosol optical depth (AOD) - that is a quantitative measure of the extinction of solar radiation by aerosol scattering and absorption between the point of observation and the top of the atmosphere. It is a measure of the integrated columnar aerosol load and the single most important parameter for evaluating direct radiative forcing [20].

Remote sensing works on the principle of the inverse problem. Different types of physical processes in the atmosphere are related to different types of absorption and scattering of light. The retrieval of aerosol parameters requires accurate forward modeling of the measurement: the absorption and the single-scattering properties of the aerosol as function of aerosol particle size, shape, chemical composition and vertical profile. With accurate forward modeling, aerosol optical depth (AOD) determined from observations of atmospheric spectral transmission and inverse modeling of AOD provides aerosol physical parameters such as, size distribution and effective refractive index.

# Chapter 2: Light scattering by atmospheric particulates

The most important source of electromagnetic energy is the sun. When this electromagnetic energy travels through the atmosphere it undergoes a complicated interaction with the atmospheric constitutes. Three fundamental interactions in the atmosphere are possible: absorption, transmission and scattering. The different scattering processes are

• Rayleigh scattering;

• Mie scattering;

• Resonant scattering;

• Florescence; and

• Raman scattering.

The first two scattering processes are elastic process in which no appreciable energy exchange takes place between the scatterer and the incident photons. Elastically scattered energy has the same wavelength as the incident radiation. It is customary to differentiate between the Rayleigh regime, in which the scatterer is much smaller than the illuminating wavelength, and the Mie regime, in which scatterer is comparable to or larger than the wavelength.

The strong dependence of the scattering and absorption interaction on particle size, shape and refractive index makes the measurement of electromagnetic scattering a power full noninvasive means of particle characterization in terrestrial remote sensing. Meaning full interpretation of remote sensing observations needs accurate quantitative knowledge of electromagnetic interaction as a function of particle physical parameters.

To do so, we adopt macroscopic approach to the problem of determining absorption and scattering of electromagnetic waves by particles. This approach appears to be quite manageable and forms the bases of the modern theory of electromagnetic scattering by small particles. Therefore, the logical point of departure is the Maxwell equations for the macroscopic field at interior points in matter using a linear optics.

The treatment of light scattering by atmospheric constituents partitioned into three consecutive steps:-

1) Computation of the far field scattering and absorption properties of an individual particle by solving Maxwell equations;

2) Computation of the scattering and absorption properties of a small volume element contain a tenuous particle collection by using the single-scattering approximation; and

3) Computation of multiple scattering by the entire atmospheric particle group by solving Radiative transfer equation.

Thus, in this chapter we carryout computation of the far field solution and extinction parameters of light scattering by individual spherical, linear, homogeneous, and isotropic particle, by solving Maxwell equations which leads to Mie scattering formulation. Consecutively extending the computation, we discuss the effective single scattering properties of particles appeared as continuous size distributions and special case of Mie scattering, that is, Rayleigh scattering. Finally, we see optical characteristics of Mie scattering.

## 2.1 Mie Theory

The solution of Maxwell's equations for the geometry of the aerosol (usually considered to be spherical) in the medium of interest (i.e. air) yields the connection between the index of refraction and the single scattering properties. That is, three properties are required to exactly specify the radiative effects of particles. The properties define the total extinction (scattering plus absorption) due to the particle, the probability an interaction results in absorption rather than scattering, and, finally, the angular distribution of scattered photons as a function of the incident angle. By convention, the properties defining the above attributes are usually specified as the extinction optical depth $\tau_e$, the single scattering albedo $\varpi$, and the asymmetry parameter $g$. These three parameters are known collectively as the single scattering properties of the particles.

These properties depend in turn on the mass, size, and composition of the particle species. A particle's chemical composition determines its index of refraction $m$. The index of refraction is a dimensionless, complex number given by $m = m_r + im_i$, where

$m_r$ - describes the scattering properties of the particles while $m_i$ - describes the absorption properties of the particles.

Mie theory predicts the optical efficiencies $Q_x$ of particles of a given size at a given wavelength. Here *x* stands for *a*, *s*, or *e* which represent the processes of absorption, scattering, and extinction, respectively. The optical efficiency for each of these processes is the ratio between a particle's effective cross-sectional area for the specified interaction (absorption, scattering, or both) with light and its geometric cross sectional area. Thus, the optical efficiencies are dimensionless and are not independent of one another. Two of the efficiency factors, usually the extinction efficiency $Q_e$ and the scattering efficiency $Q_s$, are predicted directly by Mie theory. The third efficiency factor, the absorption efficiency $Q_a$ is the residual that satisfies energy conservation $Q_a(r,\lambda) = Q_e(r,\lambda) - Q_s(r,\lambda)$. This relation states that extinction is the sum of absorption and scattering.

## 2.2 Maxwell equations

The Maxwell equations for the case that there are no charge ($\rho = 0$) and current density ($J = 0$), and to the medium which is homogeneous so that $\varepsilon$ and $\mu$ are constants. Thus, Maxwell equations reduces to [21 - 23]

$$\nabla . E_c = 0 \qquad 2.2.1a$$

$$\nabla . H_c = 0 \qquad 2.2.1b$$

$$\nabla \mathrm{X} E_c = i\omega\mu H_c \qquad 2.2.1c$$

$$\nabla \mathrm{X} H_c = -i\omega\mu E_c \qquad 2.2.1d$$

The Gaussian (cgs) system of units is used.

The coupled vector equations (2.2.1) will prove more tractable once they are reduced to coupled scalar equations. This will be accomplished by using Eqs. (2.2.1) and some vector mathematics [24].

First we take the curl of Eq. (2.2.1c) and (2.2.1d)

$$\nabla X \nabla X E_c = \nabla X\left(-i\omega\varepsilon H_c\right)$$
$$= i\omega\mu \nabla X H_c$$
$$= i\omega\mu\left(-i\omega\varepsilon E_c\right)$$
$$= \omega^2 \mu\varepsilon E_c \qquad 2.2.2a$$
$$\nabla X \nabla X H_c = \nabla X\left(-i\omega\varepsilon E_c\right)$$
$$= -i\omega\varepsilon \nabla X E_c$$
$$= i\omega\varepsilon\left(-i\omega\mu E_c\right)$$
$$= \omega^2 \mu\varepsilon H_c \qquad 2.2.2b$$

Then using curl vector mathematics [24] and Eq. (2.2.1a):

$$\nabla X \nabla X E_c = \nabla\left(\nabla . E_c\right) - \nabla .\left(\nabla E_c\right) = \omega^2 \mu\varepsilon E_c$$
$$\nabla(0) - \nabla .\left(\nabla E_c\right) + \omega^2 \mu\varepsilon E_c = 0$$
$$\nabla^2 E_c + k^2 E_c = 0 \qquad 2.2.3$$

$$\nabla^2 H_c + \nabla^2 H_c = 0 \qquad 2.2.4$$

where the derivation of (2.2.4) follows (2.2.3) and (2.2.1b). We introduce the wave number $k$ as

$$k = \omega^2 \mu\varepsilon \qquad 2.2.5$$

Thus, both the electric and magnetic fields satisfy the vector wave Eqs. (2.2.3)–(2.2.4), as well as the Maxwell equations for time-harmonic fields (2.2.1). In fact, any two-vector fields *M* and *N*, which satisfy (2.2.3) and (2.2.4), are valid electric and magnetic fields. In keeping with convention [25], we let *M* and *N* denote a candidate pair of solutions to the electro-magnetic field equations.

We shall apply a gauge transformation to simplify the Maxwell equations for a plane wave scattering from a sphere. This transformation identifies a scalar generating function, which satisfies the scalar wave equation. The problem thus reduces to identifying the

correct scalar field. Denote the scalar field by $u$ and introduce a constant vector function $c$ [25].

## Separation of Variables

We now seek a function $u$, which satisfies the scalar wave equation (the Helmholtz equation) in spherical coordinates:

$$\nabla^2 u + k^2 u = 0 \qquad 2.2.6a$$

$$\frac{1}{r^2}\frac{\partial}{\partial r}\left(r^2\frac{\partial u}{\partial r}\right)+\frac{1}{r^2\sin\theta}\frac{\partial}{\partial\theta}\left(\sin\theta\frac{\partial u}{\partial\theta}\right)+\frac{1}{r^2\sin^2\theta}\frac{\partial^2 u}{\partial\phi^2}+k^2u=0 \qquad 2.2.6b$$

The separation of variables attempts to find $u$ as the product of three independent functions—one for each radial and angular coordinate:

$$u(r,\theta,\phi)=R(r)\Theta(\theta)\Phi(\phi) \qquad 2.2.7$$

where $R(r)$, $\Theta(\theta)$ and $\Phi(\phi)$ contain the radial, polar, and azimuthally dependent components of $u$. Substituting (2.2.7) into (2.2.6b) and dividing by $R\Theta\Phi$, we obtain [25]

$$\frac{1}{\Phi}\frac{d^2\Phi}{d\phi^2}=cons.=-l^2 \qquad 2.2.8$$

$$\frac{1}{R}\frac{d}{dr}\left(r^2\frac{dR}{dr}\right)+k^2m^2r^2=cons.=n(n+1) \qquad 2.2.9$$

$$\frac{1}{\sin\theta}\frac{1}{d\Theta}\frac{d}{d\theta}\left(\sin\theta\frac{d\Theta}{d\theta}\right)-\frac{l^2}{\sin^2\theta}=cons.=-n(n+1) \qquad 2.2.10$$

The single value solution for Eq. (2.2.8) is simply

$$\Phi_m(\phi)=C_{1,m}\cos m+C_{2,m}\sin m\phi \qquad 2.2.11$$

where $C_{1,m}$ and $C_{2,m}$ are constants of integration determined by the boundary conditions. A requirement of our physical problem, Mie scattering, is that the resulting

electromagnetic fields be single-valued. In other words, a given azimuthal angle $\phi$ must be associated with only one functional value so that

$$\Phi(\phi+2\pi)=\Phi(\phi) \qquad 2.2.12$$

The symmetries involved in Mie scattering make it useful to distinguish the even and odd components of $\phi$. We note that $\cos m\phi$ and $\sin m\phi$ are symmetric and anti-symmetric, respectively, so that

$$C_{1,m}\cos m\phi = C_{1,m}\cos[(-m)\phi] \qquad 2.2.13a$$
$$C_{2,m}\sin m\phi = -C_{2,m}\sin[(-m)\phi] \qquad 2.2.13b$$

Since $\cos m\phi$ and $\sin m\phi$ are orthonormal, any azimuthal function can be decomposed into a series of these basis functions

$$\Phi(\phi)=\sum_{m=0}^{\infty} C_{1,m}\cos m\phi + C_{2,m}\sin m\phi \qquad 2.2.14$$

Eq. (2.2.10) is the associated Legendre equation and its solutions are the associated Legendre polynomials. The solutions are Legendre polynomials of degree n and order m, denoted by $P_n^m(\cos\theta)$. Legendre polynomials are usually expressed in terms of $\mu=\cos\theta$:

$$\frac{d}{d\mu}\left[(1-\mu^2)\frac{d\Theta}{d\mu}\right]\left[n(n+1)-\frac{m^2}{1-\mu^2}\right]\Theta=0 \qquad 2.2.15$$

The associated Legendre polynomials of degree *n* and order *m* which satisfy (2.2.15) are denoted by $P_n^m(\mu)$. Re-defined radial function will transform (2.2.9) into Bessel's equation. Define *Z* by

$$R=\rho^{-1/2}Z$$
$$Z=\sqrt{\rho}R \qquad 2.2.16$$

and substitute it into (2.2.9) to obtain

$$\rho^2 \frac{d^2 Z}{d\rho^2} + \rho \frac{dZ}{d\rho} + \left[ \rho^2 - \left( n + \frac{1}{2} \right)^2 Z \right] = 0 \qquad 2.2.17$$

The solutions are Bessel functions of half-integral order, $Z = Z_{n+1/2}(\rho)$

In terms of the radial coordinate $r$ and wave number $k$, the solutions are

$$R(n;r,k) = \frac{1}{\sqrt{kr}} Z_{n+1/2}(kr) \qquad 2.2.18$$

The general solution to our Helmholtz equation in spherical coordinates (2.2.5) is the product of the radial, polar, and azimuthal solutions from (2.2.17), (2.2.14), and (2.2.10), respectively

$$u(n,m;r,\theta,\phi) = \frac{1}{\sqrt{kr}} Z_{n+1/2}(kr) P_n^m(\cos\theta)\left(C_{1,m}\cos m\phi + C_{2,m}\sin m\phi\right)$$

The physical environment of Mie scattering allows us to restrict the radial solutions $Z_{n+1/2}(kr)$ to certain subsets of Bessel functions. Each cylindrical function denoted in Eq. (2.2.18) may be expressed as a linear combination of two cylindrical functions of standard type, e.g., the Bessel functions $J_{n+\frac{1}{2}}(\rho)$ and the Neumann functions $N_{n+\frac{1}{2}}(\rho)$:

$$\Psi_n = \sqrt{\frac{\pi\rho}{2}} J_{n+\frac{1}{2}}, \qquad \chi_n(\rho) = -\sqrt{\frac{\pi\rho}{2}} N_{n+\frac{1}{2}} \qquad 2.2.19$$

The functions $\Psi_n(\rho)$ are regular in every finite domain of the $\rho$ plane including the origin, where as the functions $\chi_n$ have singularities at the origin $\rho$=0 where they become infinite. Therefore, we use $\Psi_n(\rho)$ but not $\chi_n$ to represent the wave inside the sphere. On utilizing the definitions in Eq. (2.2.18) can be rewritten in the form

$$rR = c_n \Psi_n(kmr) + d_n \chi_n(kmr) \qquad 2.2.20$$

where $c_n$ and $d_n$ are arbitrary constants. Eq. (2.2.20) now represents the general solution of Eq. (2.2.9). It follows the general solution of the scalar wave Eq. (2.2.6) then can be expressed by

$$r\psi(r,\theta,\phi)=\sum\sum P_n^1(\cos\theta)[c_n\psi_n(kmr)+d_n\chi_n(kmr)]\times(a_l\cos l\phi+b_l\sin l\phi) \qquad 2.2.21$$

More over, when $c_n$ = 1; and $d_n$ = $i$, we note that

$$\psi_n(\rho)+i\chi_n(\rho)=\sqrt{\frac{\pi\rho}{2}}\,H^2_{n+\frac{1}{2}}=\zeta_n(\rho) \qquad 2.2.22$$

where $H_{n+\frac{1}{2}}$ is the half integral order Hankel function of the second kind. It has the property of vanishing at infinity in the complex plane and is suitable for the representation of the scattered wave.

## 2.3 Expansion of plane wave into spherical harmonics

For simplicity, we assume that out side the medium is vacuum ($m_{medium}$ = 1), that the material of the sphere has an index of refraction $m$, and the incident radiation is linearly polarized. We select the origin of a rectangular system of coordinates at the center of the sphere, with the positive $Z$ axis along the direction of propagation of the incident wave. If the amplitude of the incident wave is normalized to unity, the incident electric and magnetic field vectors are

$$E^i=a_x e^{-ikz}, \qquad H^i=a_y=e^{-ikz} \qquad (2.3.1)$$

where $a_x$ and $a_y$ are unit vectors along the $X$ and $Y$ axes respectively.

The electric and magnetic field vectors of the incident wave using spherical coordinate are

$$E_r^i = e^{-ikr\cos\theta}\sin\theta\cos\phi$$
$$E_\theta^i = e^{-ikr\cos\theta}\cos\theta\cos\phi$$
$$E_\phi^i = e^{-ikr\cos\theta}\sin\phi \qquad (2.3.2)$$

The first factor on the right-hand side of the above equation may be expressed in the following differentiable series of Legendre polynomials [26]:

$$H_r^i = e^{-ikr\cos\theta}\sin\theta\sin\phi,$$
$$H_\theta^i = e^{-ikr\cos\theta}\sin\phi$$
$$H_\phi^i = e^{-ikr\cos\theta}\cos\phi \qquad (2.3.3)$$
$$e^{-ikr\cos\theta}\cos\phi = \sum_{n=0}^{\infty}(-i)^n(2n+1)\frac{\psi_n(kr)}{kr}P_n(\cos\theta) \qquad (2.3.4)$$

Using the mathematical identities below

$$e^{-ikr\cos\theta}\sin\theta = \frac{1}{ikr}\frac{\partial}{\partial\theta}\left(e^{-ikr\cos\theta}\right) \qquad (2.3.5)$$
$$\frac{\partial}{\partial\theta}P_n(\cos\theta) = -P_n^1(\cos\theta), \qquad P_0^1(\cos\theta) = 0 \qquad (2.3.6)$$

Eq. (2.3.6) relates the Legendre polynomial $P_n$ with the associated Legendre polynomial $P_n^1$, to determine the potential $u$ and $v$, the first of them is ($m_{medium}$ = 1):

$$E_r^i = e^{-ikr\cos\theta}\sin\theta\cos\phi = \frac{i}{k}\left[\frac{\partial^2(ru^i)}{\partial r^2} + k^2(ru^i)\right] \qquad (2.3.7)$$

Using Eqs. (2.3.5) - (2.3.7), we have

$$e^{ikr\cos\theta}\sin\theta\cos\phi = \frac{1}{(kr)^2}\sum_{n=1}^{\infty}(-i)^{n-1}(2n+1)\psi_n(kr)P_n(\cos\theta)\cos\phi \qquad (2.3.8)$$

Taking the trial solution of Eq. (2.3.8) in a series of similar form, we obtain

$$ru^i = \frac{1}{k}\sum_{n=1}^{\infty} \alpha_n \psi_n(kr) P_n^1(\cos\theta)\cos\phi \qquad (2.3.9)$$

Upon substituting Eqs. (2.3.9) and (2.3.8) into Eq. (2.3.7) and comparing coefficients, we obtain

$$\alpha_n\left[k^2\psi_n(kr) + \frac{\partial^2\psi_n(kr)}{\partial r^2}\right] = (-i)^n(2n+1)\frac{\psi_n(kr)}{r^2} \qquad (2.3.10)$$

In Eq. (2.2.20), since $\psi_n(kr)$ become infinite at the origin through which the incident wave must pass, we may let $c_n$ = 1 and $d_n$ = 0. Hence

$$\psi_n(kr) = rR \qquad (2.3.11)$$

Comparing Eq. (2.3.10) with (2.3.8), we find

$$\alpha_n = (-i)^n \frac{2n+1}{n(n+1)} \qquad (2.3.12)$$

Utilizing the similar procedures $v^i$ can be derived. Thus, for incident waves out side the sphere, we have

$$ru^i = \frac{1}{k}\sum_{n=1}^{\infty}(-i)^n \frac{2n+1}{n(n+1)}\psi(kr)P_n^1(\cos\theta)\cos\phi,$$
$$rv^i = \frac{1}{k}\sum_{n=1}^{\infty}(-i)^n \frac{2n+1}{n(n+1)}\psi_n(kr)P_n^1(\cos\theta)\sin\phi \qquad (2.3.13)$$

For internal waves, because the function $\chi_n(kmr)$ becomes infinite at the origin, only the function $\psi_n(kr)$ may be used. Thus for internal waves we have

$$ru^t = \frac{1}{mk}\sum_{n=1}^{\infty}(-i)^n \frac{2n+1}{n(n+1)} c_n \psi_n(kr) P_n^1(\cos\theta)\cos\phi,$$
$$rv^t = \frac{1}{mk}\sum_{n=1}^{\infty}(-i)^n \frac{2n+1}{n(n+1)} d_n \psi_n(kr) P_n^1(\cos\theta)\sin\phi \qquad (2.3.14)$$

The Hankel functions expressed in Eq. (2.2.22) will show the scattered properties which vanish at infinity. Therefore, for scattered waves we have

$$ru^s = \frac{-1}{k}\sum_{n=1}^{\infty}(-i)^n \frac{2n+1}{n(n+1)} a_n \xi(kr) P_n^1(\cos\theta)\cos\phi,$$
$$rv^s = \frac{-i}{k}\sum_{n=1}^{\infty}(-i)^n \frac{2n+1}{n(n+1)} b_n \xi_n(kr) P_n^1(\cos\theta)\sin\phi \qquad (2.3.15)$$

The coefficients $a_n$, $b_n$, $c_n$ and $d_n$ have to be determined from the boundary conditions at the surface of the sphere. The conditions are that the tangential components of $E$ and $H$ be continuous across the sphere surface $r = a$, so we have

$$E_\theta^i + E_\theta^s = E_\theta^t, \qquad H_\theta^i + H_\theta^s = H_\theta^t$$
$$E_\theta^i + E_\phi^s = E_\phi^t, \qquad H_\phi^i + H_\phi^s = H_\phi^t \qquad (2.3.16)$$

Eq. (2.3.16) implies that these four expressions have to be continuous at $r = a$. Consequently,

$$\frac{\partial}{\partial r}\left[r\left(u^i + u^s\right)\right] = \frac{1}{m}\frac{\partial}{\partial r}\left(ru^t\right), \qquad u^i + u^s = mu^t$$
$$\frac{\partial}{\partial r}\left[r\left(v^i + v^s\right)\right] = \frac{\partial}{\partial r}\left(rv^t\right), \qquad v^i + v^s = v^t \qquad (2.3.17)$$

From these equations, we obtain

$$
\begin{aligned}
m\left[\psi'(ka)-a_n\xi'(ka)\right] &= c_n\psi_n'(kma)\\
\left[\psi_n'(ka)-b_n\xi_n'(ka)\right] &= d_n\psi_n'(kma)\\
\left[\psi_n(ka)-a_n\xi_n(ka)\right] &= c_n\psi_n(kma)\\
m\left[\psi_n(ka)-b_n\xi_n(ka)\right] &= d_n\psi_n(kma)
\end{aligned}
\qquad (2.3.18)
$$

where the prime denotes differentiation with respect to the argument. Upon eliminating $c_n$ and $d_n$, we obtain the coefficients for the scattered waves in the form

$$
\begin{aligned}
a_n &= \frac{\psi_n'(y)\psi_n(x)-m\psi_n(y)\psi_n'(x)}{\psi_n'(y)\xi_n(x)-m\psi_n(y)\xi_n'(x)}\\
b_n &= \frac{m\psi_n'(y)\psi_n(x)-\psi_n(y)\psi'(x)}{m\psi'(y)\xi_n(x)-\psi_n(y)\xi_n'(x)}
\end{aligned}
\qquad (2.3.19)
$$

where $x = ka$ and $y = mx$

## 2.4 The far field solutions and extinction parameters

We shall now consider the far field at very large distances from the sphere. We note that for all practical applications, all light scattering observations are normally carried out in the far-field zone. In the far field the Hankel functions denoted in Eq. (2.2.22) reduce to the form

$$
\xi(kr) = i^{n+1}e^{-ikr}, \qquad kr >> 1 \qquad (2.4.1)
$$

With this simplification Eq. (2.3.16) becomes

$$
\begin{aligned}
ru^s &\approx -\frac{-ie^{-ikr}\cos\phi}{k}\sum_{n=1}^{\infty}\frac{2n+1}{n(n+1)}a_nP_n^1(\cos\theta)\\
rv^s &\approx -\frac{-ie^{-ikr}\sin\phi}{k}\sum_{n=1}^{\infty}\frac{2n+1}{n(n+1)}b_nP_n^1(\cos\theta)
\end{aligned}
\qquad (2.4.2)
$$

$$E_r^s = H_r^s \approx 0$$

$$E_\theta^s = H_\phi^s \approx \frac{-ie^{-ikr}\cos\phi}{kr}\sum_{n=1}^{\infty}\frac{2n+1}{n(n+1)}\left[a_n\frac{dP_n^1(\cos\theta)}{d\theta}+b_n\frac{P_n^1(\cos\theta)}{\sin\theta}\right]$$

$$E_\phi^s = H_\theta^s \approx \frac{-ie^{-ikr}\sin\phi}{kr}\sum_{n=1}^{\infty}\frac{2n+1}{n(n+1)}\left[a_n\frac{dP_n^1(\cos\theta)}{\sin\theta}+b_n\frac{P_n^1(\cos\theta)}{d\theta}\right] \qquad (2.4.3)$$

The three components of the electric and magnetic field vectors in spherical coordinate (Eq. 2.2.6) are given by [25],

$$S_1(\theta)=\sum_{n=1}^{\infty}\frac{2n+1}{n(n+1)}\left[a_n\pi_n(\cos\theta)+b_n\tau_n(\cos\theta)\right]$$

$$S_2(\theta)=\sum_{n=1}^{\infty}\frac{2n+1}{n(n+1)}\left[b_n\pi_n(\cos\theta)+a_n\tau_n(\cos\theta)\right] \qquad (2.4.4)$$

We find that the radial components $E_r^s$ and $H_r^s$ may be neglected in the far-field zone. Defining two scattering functions of the form

$\pi_n(\cos\theta)=\frac{1}{\sin\theta}p_n^1(\cos\theta)$, $\tau_n(\cos\theta)=\frac{dp_n^1(\cos\theta)}{d\theta}$, we may write

$$E_\theta^s = \frac{-i}{kr}e^{-ikr}\cos\phi S_2(\theta)$$

$$-E_\phi^s = \frac{-i}{kr}e^{-ikr}\sin\phi S_1(\theta) \qquad (2.4.5)$$

These fields represent an outgoing spherical wave with amplitude and state of polarization as functions of the scattering angle $\theta$. By defining the two polarization states, parallel and perpendicular Eq. (2.4.5) becomes

$$\begin{bmatrix}E_\parallel^s\\E_\perp^s\end{bmatrix}=\frac{e^{-ikr+ikz}}{ikr}\begin{bmatrix}s_2(\theta) & 0\\0 & s_1(\theta)\end{bmatrix}\begin{bmatrix}E_\parallel^i\\E_\perp^i\end{bmatrix} \qquad (2.4.6)$$

The scattered intensity components in the far-field zone can now written in terms of the incident intensity components in the form

$$I_{\parallel}^{s} = I_{\parallel}^{i} \frac{i_2}{k^2 r^2}, \qquad I_{\perp}^{s} = I_{\perp}^{i} \frac{i_1}{k^2 r^2} \tag{2.4.7}$$

where $i_1(\theta) = |S_1(\theta)|^2$, $i_2(\theta) = |S_2(\theta)|^2$ and they are called the intensity functions for the perpendicular and parallel components, respectively. In the far-field zone, we would like to evaluate the reduction of the incident energy due to absorption and scattering of light by a sphere. For this purpose, we consider incident light polarized linearly in the perpendicular direction. From Eq. (2.4.6) the scattered electric field is given by

$$E_{\perp}^{s} = \frac{e^{-ikr+ikz}}{ikz} S_1(\theta) E_{\perp}^{i} \tag{2.4.8}$$

Consider a point $(x, y, z)$ in the forward direction, i.e. $\theta = 0$. In the far field since $x.y << z$, we have in the forward direction

$$r = \left(x^2 + y^2 + z^2\right)^{\frac{1}{2}} \approx z + \frac{x^2 + y^2}{2z} \tag{2.4.9}$$

Upon superimposing the incident and scattered electric fields in the forward direction, we obtain

$$\left|E_{\perp}^{i} + E_{\perp}^{s}\right| \approx \left|E_{\perp}^{i}\right|^2 \left\langle 1 + \frac{S_1(0)}{ikz} e^{-ik\left(\frac{x^2+y^2}{2z}\right)} \right\rangle \tag{2.4.10}$$

The far field combined flux density in the forward directions then is proportional to

$$\left|E_{\perp}^{i} + E_{\perp}^{s}\right|^2 \approx \left|E_{\perp}^{i}\right|^2 \left\langle 1 + \frac{2}{kz} \mathrm{Re}\left[ \frac{S_1(0) e^{-ik\left(\frac{x^2+y^2}{2z}\right)}}{i} \right] \right\rangle \tag{2.4.11}$$

Integrating the combined flux density over the cross section area of a sphere whose radius is $r = a$, we obtain the total power combined:

$$\frac{1}{\left|E_{\perp}^{i}\right|^{2}} \iint \left|E_{\perp}^{i} + E_{\perp}^{s}\right|^{2} dxxy = \pi a^{2} - \sigma_{e} \tag{2.4.12}$$

where the first term on the right-hand side of Eq. (2.4.12) represents the cross section of area of the sphere. The physical interpretation of the second term $\sigma_e$ is that the total light received in the forward direction is reduced by the presence of the sphere, and the amount of the reduction is as if an area $\sigma_e$ of the object had been covered up. The double integral over $dxdy$ by which $\sigma_e$ is defined contains two Fresnel integrals, and if the limits are assumed to extend to $\infty$, we get

$$\int_{-\infty}^{\infty}\int_{-\infty}^{\infty} e^{-ik\left(\frac{x^{2}+y^{2}}{2z}\right)} dxdy = \frac{2\pi z}{ik} \tag{2.4.13}$$

Thus, the extinction cross section is $\sigma_e = \frac{4\pi}{k^{2}} \mathrm{Re}[S(0)]$.

The two amplitude functions in the forward directions reduce to $S_1(0) = S_2(0)$:

$$S(0) = \frac{1}{2}\sum_{n=1}^{\infty}(2n+1)(a_n + b_n). \tag{2.4.14}$$

The fact that there is only one $S(0)$ is because of the symmetry of the forward scattering in which the extinction is independent of the state of polarization of the incident light. It should be noted that Eq. (2.4.14) is valid when the sphere is isotropic and homogeneous. The extinction efficiency for a sphere with a radius of $r = a$ is

$$Q_e = \frac{\sigma_e}{\pi a^{2}} = \frac{2}{x^{2}}\sum_{n=1}^{\infty}(2n+1)\mathrm{Re}(a_n + b_n) \tag{2.4.15}$$

where $x = ka$: $x = \frac{2\pi a}{\lambda}$ is called the size parameter.

The flux density of the scattered light in an arbitrary direction is given by

$$F(\theta,\phi)=\frac{F}{k^2r^2}\left[i_2(\theta)\cos^2\phi+i_1(\theta)\sin^2\phi\right] \tag{2.4.16}$$

with $F_0$ = 1 (unit amplitude). The total flux (or power) of the scattered light is therefore

$$f=\int_0^{2\pi}\int_0^{\pi}F(\theta,\phi)r^2\sin\theta d\theta d\phi \tag{2.4.17}$$

where $\sin(\theta)d\theta d\phi$ is the differential solid angle $d\Omega$ and $r^2d\Omega$ depends the differential area. Hence, the scattering cross section may be defined as

$$\sigma_s=\frac{f_s}{F_0}=\frac{\pi}{k^2}\int_0^{\pi}[i_1(\theta)+i_2(\theta)]\sin\theta d\theta \tag{2.4.18}$$

In a similar way, we define the scattering efficiency for a sphere by

$$Q_s=\frac{\sigma_s}{\pi a^2}=\frac{1}{x^2}\int_0^{\pi}[i_1(\theta)+i_2(\theta)]\sin\theta d\theta \tag{2.4.19}$$

Using the orthogonal and recurrence properties of the associated Legendre polynomials [22-25], the scattering efficiency can be evaluated with the help of

$$Q_s=\frac{2}{x^2}\sum_{n=1}^{\infty}(2n+1)\left(|a_n|^2+|b_n|^2\right) \tag{2.4.20}$$

Finally, the absorption cross section and efficiency of a sphere can be calculated from

$$\sigma_a=\sigma_e-\sigma_s\ ,\qquad Q_a=Q_e-Q_s$$

where $\sigma_a=\frac{\pi}{k^2}\left[\sum_{n=1}^{\infty}(2n+1)(-1)^n(a_n-b_n)\right]^2$ (2.4.21)

and

$$Q_a = \frac{1}{x^2}\left[\sum_{n=1}^{\infty}(2n+1)(-1)^n(a_n - b_n)\right]^2 \qquad (2.4.22)$$

## 2.5 Effective Single Scattering Properties

In nature, particles are not monodisperse rather they have continuous size distributions. Therefore, the single scattering properties of each particle size must be appropriately weighted and combined into the net or effective single scattering properties of the entire size distribution. These effective properties are the optical properties of an infinitely narrow spectral region. The size distribution ($n(r,z)$[$m^{-3}$ $m^{-1}$]), describes the rate of change of particle concentration with particle size and it is a function of height, which we denote by *z*:

$$n(r) = \frac{dN(r)}{dr} \qquad 2.5.1$$

The total particle concentration is the integral of the number size distribution:

$$N_0 = \int_0^{\infty} n(r)dr \qquad 2.5.2$$

$N_0$, has dimension of [$m^{-3}$], particle number per unit air volume. The total cross-sectional area $A_0$ is the integral of the cross-sectional area weighted by the size distribution:

$$A_0 = \int_0^{\infty} \pi r^2 n(r)dr \qquad 2.5.3$$

$A_0$, has dimension of [$m^2$ $m^{-3}$], particle area per unit air volume.

Effective efficiencies $Q_x^E$ of particles of a given size distribution at a given wavelength is given by

$$Q_x^E = \frac{1}{A_0}\int_0^\infty \pi r^2 Q_x(r,\lambda)n(r,z)dr \qquad 2.5.4$$

The effective efficiencies, like the fundamental optical efficiencies, are dimensionless.

The effective cross sections are the fundamental optical cross sections integrated over the size distribution:

$$\sigma_x^E = A_0 Q_x^E = \int_0^\infty \pi r^2 Q_x(r,\lambda)n(r,z)dr \qquad 2.5.5$$

The dimensions of the effective cross-sections are, [$m^2$ $m^{-3}$], particle area per unit air volume. Hence, they are also known as the volume absorption, scattering, and extinction coefficients. These units are usually expressed as [$m^{-1}$].

## 2.6 Rayleigh scattering

When the particle size is much smaller than the incident wavelength (< 0.003), the scattering is called Rayleigh scattering. Scattering can be explained in terms of the electromagnetic theory. The electric field of the incident wave sets in oscillation of the electric charges in the particle. When the size of the particle is small than the wavelength of the incident radiation an electric dipole is set up and the scattering is symmetric because of an electric dipole radiates equal amount of fluxes in both forward and backward directions (Rayleigh scattering).

Rayleigh scattering is a special case of Mie scattering. Thus, for modeling Rayleigh scattering following the above result in Mie scattering i.e. Eq. (2.3.19) under the approximation of the particle size is much smaller than the incident wave length (< 0.003), $n = m = m_r$ (the complex refractive index equal to the real part) and $m_r$ is not greater than one. Then the expansion of scattered wave expansion coefficients, them selves as the power of $x$ [25]:

$$a_1 = \frac{2i(n^2-1)^2(x^3)}{3(n^2+2)^2} \qquad 2.6.1$$

$$a_2 = \frac{i(n^2-1)(x^5)}{15(2n^2+3)} \qquad 2.6.2$$

$$b_1 = \frac{-i(n^2-1)(x^5)}{45} \qquad 2.6.3$$

where $x = \frac{2\pi a}{\lambda}$ is the size parameter.

The above expansion converges to Raleigh scattering cross section, so the leading terms in the expression of amplitude function dominated by the first term $a_1$ (Eq. 2.6.1), then the scattering cross section (the Raleigh scattering cross section per molecule) becomes

$$C_{scat}(\theta) = \frac{8\pi^4 a^6 (n^2-1)^2 (\cos^2(\theta)+1)}{r^2 \lambda^4 (n^2+2)^2} \qquad 2.6.4$$

If Eq. (2.6.4) is written in terms of the molecular volume `$V$` instead of radius `$a$` the scattering cross section per molecule becomes

$$C_{scat}(\theta) = \frac{9\pi^2 V^2 (n^2-1)^2 (\cos^2(\theta)+1)}{2r^2 \lambda^4 (n^2+2)^2} \qquad 2.6.5$$

Then the total energy scattered in all direction or the total scattering cross section obtained by the integration of Eq. (2.6.5) is

$$C_{scat} = \int_0^{2\pi} \int_0^{\pi} C_{scat}(\theta) r^2 \sin(\theta) d\theta d\phi \qquad 2.6.6$$

$$C_{scat} = \frac{24\pi^3 V^2 (n^2-1)^2}{\lambda^4 (n^2+2)^2} = \frac{24\pi^3 (n^2-1)^2}{\lambda^4 N^2 (n^2+2)^2} \qquad 2.6.7$$

where $N$ is the number of molecules having a molecular volume `$V$` per unit volume.

## 2.7 Optical characteristics of Mie scattering

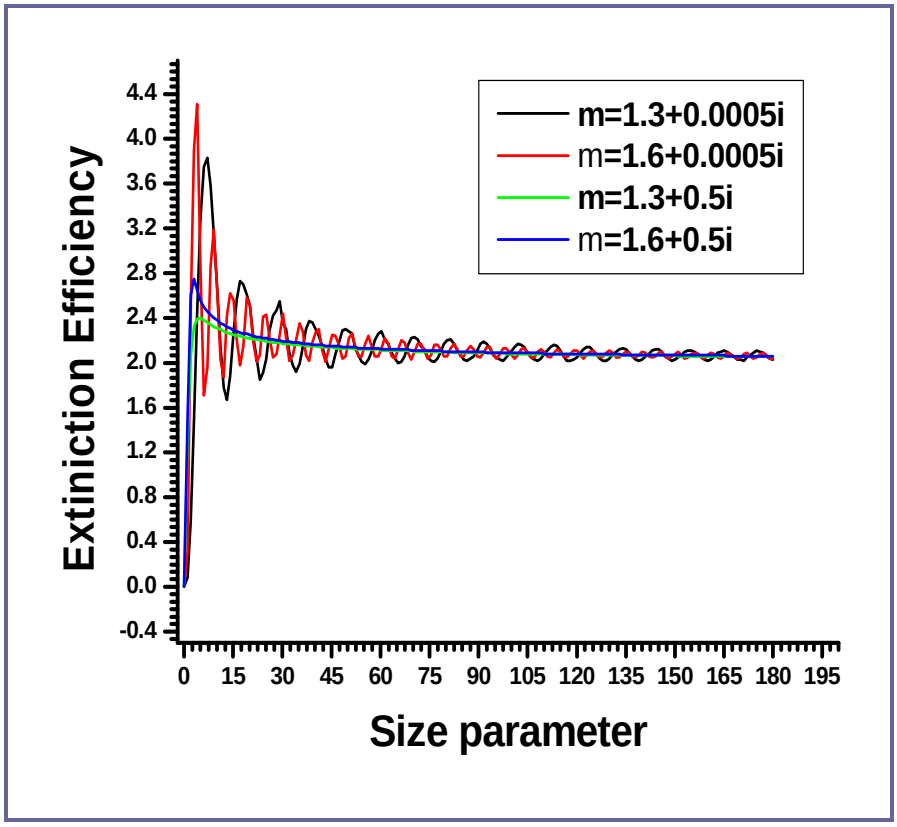


Figure 2.1: Extinction efficiency dependence on size parameter and complex refractive index.

Extinction efficiency depends on size parameter: The ratio of the circumference of the particle to the wavelength ( $x = \frac{2\pi a}{\lambda}$ ) and Complex Refractive Index. For all complex refractive indexes, maximum extinction occurs when the radius of the particle is comparable with incident wavelength. Extinction efficiency converges to 2 when the size parameter increases.

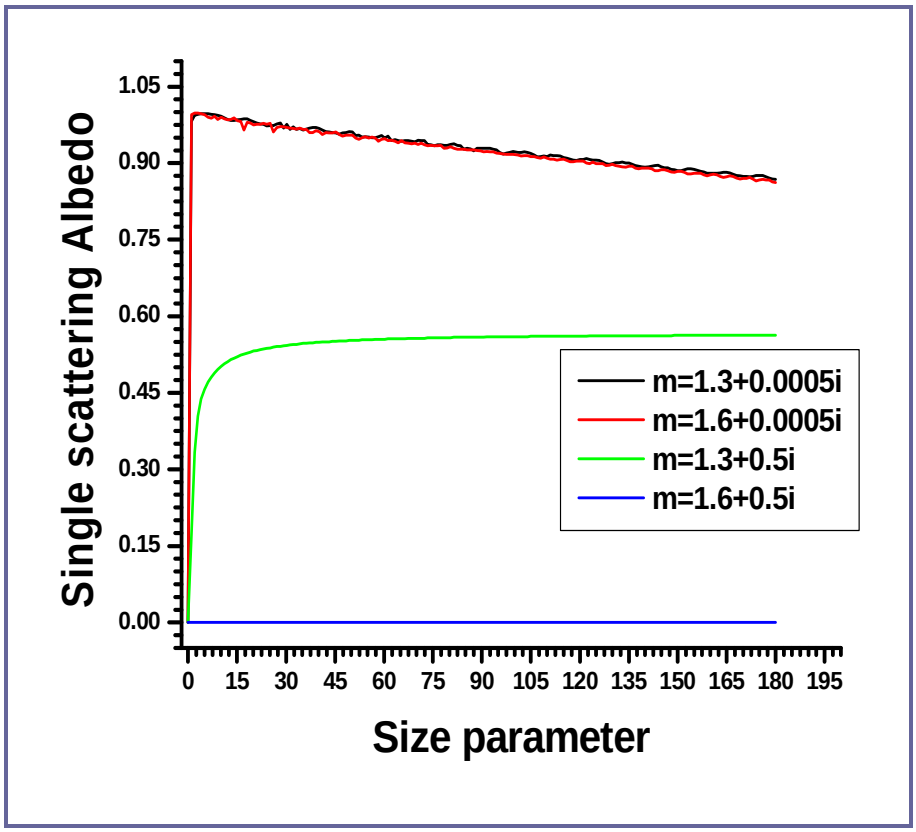


Figure 2.2: Single scattering albedo dependence on size parameter and complex refractive index.

Single scattering albedo: the ratio of the scattering coefficient to the extinction coefficient; $\omega_0 = \frac{\sigma_s}{\sigma_e}$ in Fig. 2.2 clearly shows that rather than size parameter single scattering albedo highly depends on complex refractive index. It shows that $\omega_0$ approaches one for non-absorbing aerosols and zero for absorbing aerosols.

# Chapter 3

# Direct component of solar radiation

Energy from the Sun reaching the Earth drives almost every known physical and biological cycle in the Earth-atmospheric system. Following Planck's law, solar radiation can be described as radiation emitted from a black body at a temperature of about 6000 K. Consequently, the solar component comprises of radiation from the gamma rays to the infrared spectral range. Only 0.4% of the energy of solar radiation is emitted at wavelengths above $5\,\mu m$. The spectral distribution of the Sun's radiation as observed from Earth's orbit is shown in Fig.3.1. This curve of the flux above the Earth's atmosphere at the mean Sun–Earth distance of 1AU is referred to as the solar spectral irradiance. Its integral over wavelength constitutes of solar spectral irradiance at the top of the Earth's atmosphere on a surface oriented perpendicular to the Sun's rays is referred to as total solar irradiance or solar constant. The generally accepted solar constant of 1368 $W/m^2$ is a satellite measured yearly average [27].

By making solar spectral radiation calculations and examining radiation measurements using passive remote sensors such as radiometers, we can gain a better understanding of many physical cycles and concepts associated with the Earth-atmospheric system.

In this chapter, we give briefly general over view of solar spectral irradiance transmission through the earth's atmosphere, theory of direct- solar spectral irradiance measurements, sun photometer data retrieval and retrieval of microphysical properties of aerosols from aerosol optical property: AOT.

## 3.1 General Information on solar radiation fluxes in the atmosphere

The solar spectral energy available at top of the atmosphere as it passes through the atmosphere under goes complicated transformation all the way from the outer boundary of the atmosphere to the earth's surface: a portion is absorbed, a portion is scattered. The scattered part is partly diffused back to space, while the remainder reaches the ground as

sky radiation. The solar radiation reaching an observer on the ground is only a portion of the solar radiation entering the Earth's atmosphere.

The UV-region which call in to play the electronic excitation and transfer interaction mechanism, so that, the gases opacity in this spectral region of solar radiation mainly taken by those high-altitude ozone gases, which efficiently limit the solar radiation that reach the ground in appreciable quantities [28].

The visible and near-IR, which call in to play electronic and vibration energy transitions interaction mechanisms, many endless gaseous absorption, water vapor and others, usually occurs at well-defined spectral lines. In addition, suspended particulates (aerosols), cloud drops and others make absorption in this spectral region [28].

While scattering by molecules and by aerosols in suspension in the atmosphere is responsible for the continuous extinction, there are also other contributors. The scattering by the gaseous components of the atmosphere and particulates having physical dimensions small compared to the spectral wavelength are known as Rayleigh scatterers, they dominate the scattering pattern under cases of a very clear and haze-free atmosphere.

The scattering by atmospheric components having size comparable to the spectral wavelength or larger are known as Mie scatterers. For turbid or slightly turbid atmosphere in blue and UV range, the Mie scattering is at least equally important as Rayleigh scattering. For this atmosphere, in the visible and near-IR, the scattering process is dominated by Mie scattering.

Because of the scattering of radiant energy we observe at the surface level not only direct solar radiation in the form of parallel beam of the sun's ray, but also diffused radiation falling from every point of the sky. Direct solar radiation and diffused radiation together constitute global radiation.

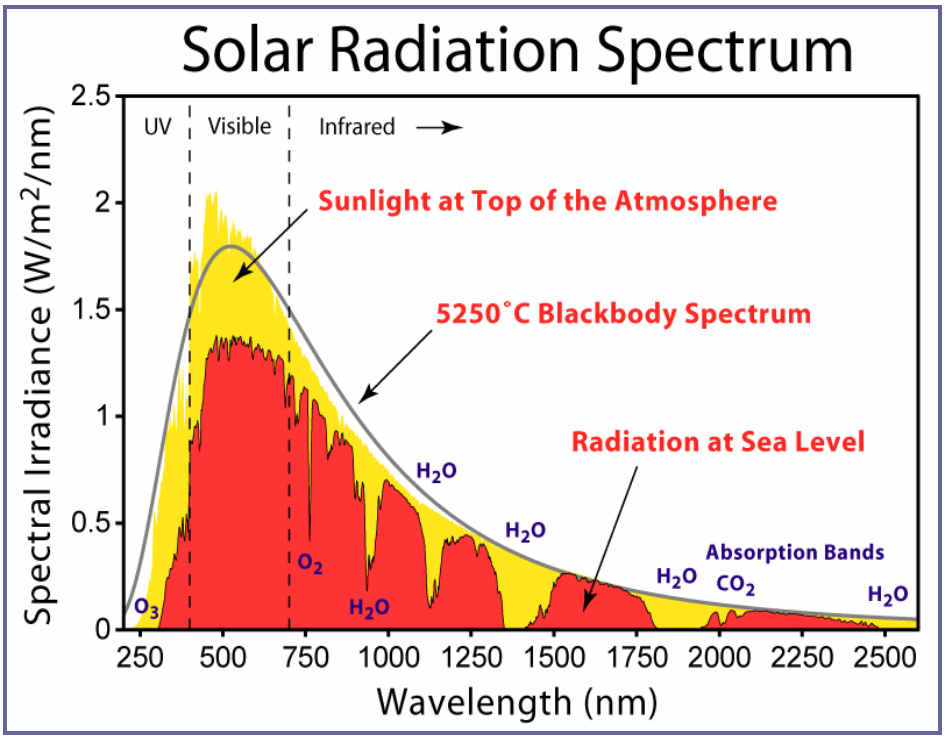


Figure 3.1: Solar spectral irradiance at the top of the atmosphere (extraterrestrial) and at surface see-level (taken from http://eosweb.larc.nasa.gov/cgi-bin/sse/daily.cgi).

Even though the Sun is not a perfect black body, black body emissions at a given temperature fairly estimate solar emission spectrum at the top of the atmosphere. And this has been used to estimate the sun temperature and the abstraction of solar spectral energy due to the atmosphere is shown in Fig. 3.1.

So up on reaching the earth surface the global radiation is partly reflected by the earth surface and the unreflected part of global radiation is absorbed by the earth's surface. The absorbed global radiation then heats the surface. The heated surface becomes source of the thermal radiation, which is directed to the atmosphere. The atmosphere is heated in the course of heat exchange with the earth's surface, and as a result, it emits thermal radiation into surface and space.

A blackbody temperature for the atmosphere-earth system is 255K. At this temperature, a blackbody emits only 0.4% of its radiation at wavelengths below $5\,\mu m$ [27], i.e. source of radiation from $0.3\,\mu m$ - $4\,\mu m$, contributed only from the solar radiation and from $4\,\mu m$ - $1\,cm$. The radiation that comes from the terrestrial radiation dominates that of

solar radiation in those long wavelength rang (see Fig.3.2, which shows that the solar and earth spectrum has nearly no over lap) [29].

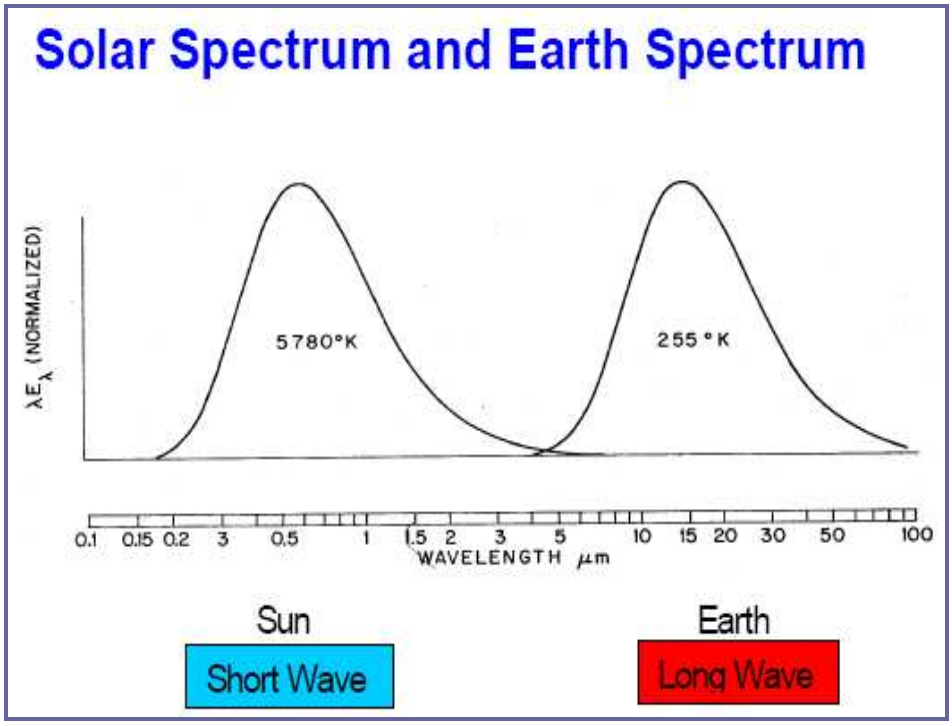


Fig.3.2 The solar and earth spectrum

## 3.2 Theory of direct-solar spectral irradiance measurements

Sun photometers are automated instruments incorporating a Sun-tracking unit, an appropriate optical system, a spectrally filtering device, a photo detector, and a data acquisition system. It measures direct solar irradiance by first pointing the collimator toward the approximate position of the sun (provided it is aligned properly) based on an in-built program that takes into account the time of the year and the coordinates of the location. Then detector positions the sun at the center of the fields of view of the collimators. The filter wheel rotates in front of the detector to obtain a measurement sequence.

In general, if we want to know how radiation will be attenuated in the atmosphere by aerosols, gases and/or clouds we need to solve a radiation transfer equation. Using plane-parallel particulate medium illuminated from above by a parallel beam representing solar radiation and stratified atmosphere: all atmospheric properties, e.g., temperature, density, vary only in the vertical standard atmospheric model.

The differential form of the equation for radiative transfer is:

$$\frac{dI_\lambda}{dr} = -\sigma_{ext}(\lambda, r) I_\lambda + \int_0^{\pi} \int_0^{2\pi} \sigma_{scat}(\lambda, r, \theta', \phi') I_\lambda \sin\theta' d\theta' d\phi' \qquad 3.2.1$$

where $\sigma_{scat}(\lambda, r, \theta', \phi')$ is the spectral value of the directional scattering coefficient of atmospheric constituents at altitude *r*, $\sigma_{ext}(\lambda, r)$ is the spectral value of extinction coefficient of atmospheric constituents at altitude *r*, $I_\lambda$ is the observed direct and diffused solar spectral irradiance at altitude *r*, $r, \theta', \phi'$, and $\lambda$ are altitude, zenith and azimuth directional scattering angles in spherical coordinate and wavelength of solar radiation respectively.

Since the contribution of multiple scattering within the small field of view of the sun-photometer is negligible: the measured radiant flux is due to a combination of what is emitted by the Sun (i.e. the solar extraterrestrial radiance) and the effect of the atmosphere. The Beer-Lambert law for the atmosphere gives the link between these quantities.

If $I_{0_\lambda}$ is the intensity of a narrow beam of sunlight radiation at the top of the atmosphere and $I_\lambda$ is the observed direct solar spectral irradiance at Earth's surface after a given path is given by

$$I_\lambda = \frac{I_{o\lambda}}{\gamma^2} e^{\left[-m\left(\tau_{\lambda a}+\tau_{\lambda g}+\tau_{\lambda NO_2}+\tau_{\lambda \omega}+\tau_{\lambda O_3}+\tau_{\lambda r}\right)\right]} = I_{o\lambda} e^{[-\tau_\lambda]} \qquad 3.2.2$$

where $\tau_\lambda = m\left(\tau_{\lambda a} + \tau_{\lambda g} + \tau_{\lambda NO_2} + \tau_{\lambda \omega} + \tau_{\lambda O_3} + \tau_{\lambda r}\right)$ is total spectral optical depth for a slant path of the atmosphere. This expresses the quantity of light removed from a beam by scattering or absorption during its path through a medium.

Each $\tau_{\lambda x}$ corresponds to the spectral optical depth for vertical path from Earth's surface to outer space and $m(\tau_{\lambda x})$ is the spectral optical depth for a slant path from the observer's altitude to outer space. Whose subscript identifies the source of the absorption or scattering it describes:

*a* refers to aerosol (that absorb and scatter);

*g* are uniformly mixed gases (mainly $CO_2$ and $O_2$ which only absorb);

*$NO_2$* Nitrogen dioxide mainly due to urban pollution (absorption only);

*w* is water vapor absorption;

*$O_3$* Ozone (absorption only);

*r* is Rayliegh scattering from molecular oxygen ($O_2$) and nitrogen ($N_2$) (responsible for the blue color of the sky) and

$m$ is the optical mass or air mass factor.

$\gamma = \frac{R}{R_0}$ is the ratio of the earth-sun distance to its mean value, in units of AU, at the time you make a measurement; it is a function of the date on which a measurement is made and it is used to correct the constant $I_{0\lambda}$ a sun photometer would see at the time of a measurement. It is given by

$$\gamma = 1 - \varepsilon \cos\left(\frac{2\pi(J-4)}{365.3}\right) \qquad 3.2.3$$

where the orbit eccentricity $\varepsilon$ = 0.01673 and $J$ is Julian day.

The air mass $m$ (also called atmospheric mass) is defined as the number of times one has, along the line of sight, the quantity of air seen in the direction of the zenith (at sea level). $m$ depends on the path of the light ray and is a function of the earth's curvature and atmospheric refraction. For a plane-parallel atmosphere it is determined as

$$m(\theta) = \sec\theta \ , \qquad \text{for } \theta \le 70^0, \qquad \text{with in 1\%} \qquad 3.2.4$$

At large zenith distances, the curvature of the atmosphere, the atmospheric refraction and, the variation of atmospheric density with height complicate the exact calculation of the air mass. As a result Eq. (3.2.4) is modified [30] as

$$m(\theta) = \sec\theta\left[1 - 0.0012\left(\sec^2\theta - 1\right)\right] \qquad 3.2.5$$

## 3.3 Inverse modeling of sun photometer observation

The inversion of the solar radiances measured by the sun-photometer to retrieve the aerosol optical thickness values is based on Eq. (3.2.2).

## Transmittance of the Earth's atmosphere

The ability of the atmosphere to allow radiation to pass through it is referred to as its transmissivity, and varies with the wavelength type of the radiation. The monochromatic transmittance or transmission coefficient of the Earth's atmosphere due to direct radiation can be written as:

$$T_\lambda = \frac{\gamma^2 I_\lambda}{I_{o\lambda}} = e^{\left[-m\left(\tau_{\lambda a} + \tau_{\lambda g} + \tau_{\lambda NO_2} + \tau_{\lambda \omega} + \tau_{\lambda O_3} + \tau_{\lambda r}\right)\right]} = e^{\left[-\tau_\lambda\right]} \qquad 3.3.1$$

where $T_\lambda$ is monochromatic transmittance or transmission coefficient of the Earth's atmosphere. It varies with the composition of the atmosphere.

$T_\lambda$ of the atmosphere can be divided into several components, for clear sky (cloudless) atmosphere, ascribed to molecular monochromatic transmittance and aerosols monochromatic transmittance:

$$T_\lambda = \frac{\gamma^2 I_\lambda}{I_{o\lambda}} = e^{\left[-m\left(\tau_{\lambda a} + \tau_{\lambda g} + \tau_{\lambda NO_2} + \tau_{\lambda \omega} + \tau_{\lambda O_3} + \tau_{\lambda r}\right)\right]} = e^{\left[-m\tau_{\lambda_m}\right]}.e^{\left[-m\tau_{\lambda_a}\right]} = e^{\left[-\tau_{\lambda A}\right]}.e^{\left[-\tau_{\lambda M}\right]}$$

$$T_\lambda = T_{m\lambda}.T_{a\lambda} \qquad 3.3.2$$

where $T_{m\lambda} = e^{[-\tau_{\lambda M}]}$ is molecular monochromatic transmittance ascribed to molecular (Rayleigh) scattering and gaseous absorption and $\tau_M$ is the molecular optical depth for a slant path of the atmosphere.

$T_{a\lambda} = e^{[-\tau_{\lambda A}]}$ is aerosols monochromatic transmittance ascribed to aerosols scattering and absorption and $\tau_{\lambda A}$ is the aerosol spectral optical depth for a slant path of the atmosphere.

Using Eqs. (3.3.1) and (3.3.2) total spectral optical depth of the atmosphere ($\tau_\lambda$) is defined by the following equation

$$\tau_\lambda = -\ln T_\lambda = -\ln\left(\frac{\gamma^2 I_\lambda}{I_{o\lambda}}\right)$$

$$\tau_\lambda = -\ln T_{m\lambda} - \ln T_{a\lambda} = \tau_{\lambda M} + \tau_{\lambda A} \qquad 3.3.3$$

From the total spectral optical depth of the atmosphere by correcting the contribution of Rayleigh scattering and gaseous absorption using model values or other system data set we can determine the aerosol spectral optical thickness (AOT). If a sun-photometer measures light intensity such that the voltage signal produced by the instrument is directly proportional to intensity, then the same as Eq. (3.3.1) can be modified as

$$V_\lambda = \frac{V_{o\lambda}}{\gamma^2} e^{\left[-m\left(\tau_{\lambda a}+\tau_{\lambda g}+\tau_{\lambda NO_2}+\tau_{\lambda \omega}+\tau_{\lambda O_3}+\tau_{\lambda r}\right)\right]} = V_{o\lambda} e^{[-\tau_\lambda]} \qquad 3.3.4$$

The voltage $V_{0\lambda}$, the extraterrestrial constant, is the voltage when the sun-photometer would see if it were pointed at the sun just outside the earth's atmosphere when the earth is 1 astronomical unit (AU) from the sun.

The calibration constant (which depend on sensitivity of the sun-photometer detector) is determined for the instrument to convert the solar extraterrestrial spectral energy distribution (watts per square meter) to an equivalent mill volt signal.

This calibration value depends primarily on the wavelength at which your sun-photometer detects light and on the distance between Earth and the sun. This distance varies slightly because Earth follows a slightly elliptical, rather than a circular, path around the sun.

The voltage $V_\lambda$ is what you record when you point your sun photometer at the sun, minus the dark voltage. Then, solving for $\tau_{\lambda A}$ using Eq. (3.3.3) gives

$$\tau_{\lambda A} = \left[\ln V_{0\lambda} - \ln\left(\gamma^2 V_\lambda\right) - \tau_M\right] \qquad 3.3.5$$

## 3.4 Rretrieval of aerosol refractive index and particle size distribution from ground-based measurements of direct solar radiation.

The principle of the inverse problem: the object or phenomenon of interest (the state) may not be directly measured, there exists some other variable that can be detected and measured (the observation), which may be related to the object of interest through the physical laws that give the processes.

The physical laws can be put together to describe the processes in full or approximately. This description or model is formulated in a manner suitable to handle it using computer.

Ground-based sun-photometer observation of direct solar radiation is a tool for providing data on aerosol optical properties. Spectral transmission measurements provide an optical source of aerosol information, which can be inverted for retrieval of microphysical properties (particle size distribution and refractive index).

Since aerosol radiative properties depend on factors such as aerosol particle size, shape, chemical composition (which determines refractive index), a forward model must take such factors into account. Assuming the particles are spherical allows computation of radiative properties from Mie theory (section 2.1).

These optical depths retrieved from the sun photometer at solar spectral regime were utilized to retrieve columnar aerosol size distribution by applying the constrained linear inversion method [32, 33]. Having obtained AOD at different wavelengths, aerosol size

distribution (ASD) can be determined by following the inversion scheme suggested by [31-33], which connects the AOD and ASD by

$$\tau_A(\lambda) = \int_0^\infty \pi r^2 Q_{ext}(x, \lambda, m) n_c(r) dr \qquad 3.4.1$$

where $r$ is the particle radius, $m$ is the complex refractive index of aerosol particles; $Q_{ext}(r, \lambda, m)$ is the Mie extinction efficiency parameter, $n_c(r)$ is the columnar aerosol size distribution (i.e., the number of particles per unit area per radius interval in a vertical column through the atmosphere). In the complex refractive index ($m = m_r + im_i$), the real quantity represents contribution due to particulate scattering while the imaginary quantity denotes the particles' absorption.

Since $n_c(r)$ cannot be written analytically, a numerical approach is followed to separate $n_c(r)$ into two parts as $n_c(r) = h(r).f(r)$, where $h(r)$ is rapidly varying function with $r$ and $f(r)$ is slowly varying. Hence Eq. (3.4.1) is modified as

$$\tau_A(\lambda) = \sum_{j=1}^{q} \int_{r_j}^{r_{j+1}} \pi r^2 Q_{ext}(x, \lambda, m) h(r) f(r) dr \qquad 3.4.2$$

In Eq. (3.4.2), the quadrature error will be less if $f(r)$ is assumed to be constant. In that case, a system of linear equations results, which may be written as

$$\tau_A(\lambda) = Af(r) + \varepsilon \qquad 3.4.3$$

where $A = \int \pi r^2 Q_{ext}(x, \lambda, m) h(r) dr$ and $\varepsilon$ is an error which arises due to deviation between the measured $\tau_A$ and theoretical $(\tau_A = \sum A_{ij} f_i)$. Initially, Junge exponent $(\upsilon)$ is computed from the wavelength dependence of aerosol optical depth and used as zero-order weighting function $h^0(r)$. By using $h^0(r)$ as an initial guess, first order $f^{(1)}$ values are evaluated using

$$f^{(1)} = \left(A^T S_\varepsilon^{-1} A + \gamma H\right)^{-1} A^T S_\varepsilon^{-1} \tau_A \qquad 3.4.4$$

where $\gamma$ is non-negative Lagrangian multiplier and $S_\varepsilon$ is the measured covariance matrix, $H$ is a mean diagonal matrix and superscript $T$ denotes matrix transposition. This iteration procedure is repeated until the observed $\tau_A$ comes closer to the re-computed $\tau_A$. Since the optical depth is not linearly related with the solution vector $f_i$, we have to use non-linear retrieval procedures given below:

$$f_{n+1} - f_n = \left(A^T A + \gamma H\right)^{-1} A^T \left(\tau_{measured} - \tau_{simulated}\right) \qquad 3.4.5$$

In order to retrieve particle size distribution of aerosol and to estimate simultaneously the effective refractive index, we choose aerosol refractive index having a minimum $\chi^2$ error between simulated and measured optical thickness values:

$$\chi^2 = \sum_{i=1}^{n} \left(\tau_{measured}(\lambda_i) - \tau_{simulated}(\lambda_i)\right)^2$$

# Chapter 4: Pyrheliometer

The Passive instruments detect natural energy (radiation) that is emitted or reflected by the object or surrounding area being observed. Sunlight is the most common external source of radiation sensed by passive instruments. Using a passive remote sensor (radiometer) the down welling direct beam of sunlight irradiance is most accurately measured by a normal incidence pyrheliometer (NIP).

The measured radiation data at discrete wavelength provide total column atmospheric aerosol optical depth at these wavelength bands. Measurements of aerosol optical thickness at more than one wavelength are used for retrieving the aerosol size distribution and the complex refractive index [32, 33 and 34].

Knowing the size distribution and complex refractive index together with observable relationships between aerosols and temperature, cloud cover, relative humidity, and precipitation, helps identify the source of the aerosols. Several parameters of aerosols could be produced using Mie scattering calculation and provided to the atmospheric input data needed for the radiative transfer model calculations.

Information on aerosol is needed to monitor the present distribution of aerosols, to understand the local and global distribution and variability of aerosols, to track events that alter aerosol concentrations, for climate studies: a better understanding of Earth's climate and how it is changing and comparison with satellite data.

So in this chapter we discus in detail about pyrheliometer and especially about pyrheliometer, which we constructed in department of physics at AAU: its component specifications, concepts used for effective wavelength, absorptions and analysis.

## 4.1 Pyrheliometers

Pyrheliometer is a general term for the class of actinometer instrument, designed specifically to measure the intensity of direct solar radiation. The instrument consists of a radiation-sensing element enclosed in a casing that is closed except for a small aperture through which the direct solar rays enter. A field of view limited to 5 °. This is achieved by the shape of the collimation tube, with precision apertures, and the detector design. Incorporating Passive Solar Tracker (PST) provide sighting arrangement for aiming the

pyrheliometer directly at the sun continuously throughout the day. This means the instrument is always aimed directly at the sun. That is, when a Pyrheliometer is placed some where within the Earth's atmosphere, pointing the collimator toward the approximate position of the sun (provided it is aligned properly) based on an in-built program that takes into account the time of the year and the coordinates of the location that are input to control box prior to operation. A detector then positions the sun at the center of the fields of view of the collimators by using a feedback control loop. The filter wheel rotates in front of the detector to obtain a spectral measurement sequence [29, 34, and 35].

In order to study the characteristics of atmospheric aerosols, various properties and their time variation using passive remote sensing techniques principles; so based on the above and the theory of direct solar radiation measurement (chapter 3) we have constructed a simple Pyrheliometer at AAU.

## 4.2 Design of pyrheliometer and Passive solar tracker (PST)

Figure 4.1: Home made pyrheliometer at AAU.

**Collimator tube**

The intensity of radiation from the circumsolar sky is function of solar elevation, station altitude and atmospheric conditions. One of the major problems in measuring the direct solar radiation is the amount of circumsolar sky seen by a Pyrheliometer detector. It is impossible to eliminate the circumsolar sky radiation completely from the measurements because of the finite dimensions of the components, the practical difficulty of exact orientation of the instrument and the inability to define the solar disk precisely.

Having taken these facts into account, we design our collimator tube according to the recommendation of the international radiation commission standard geometry of Pyrheliometer tube [29].

If `$R$` is the radius of the field stop, `$r$` the radius of the aperture and `$l$` the distance between the two radii, international radiation commission recommends that the pyrheliometers should have a slope angle $\alpha$ and the ratio of $\frac{l}{r}$ to be $1^o \le \alpha \le 2^o$, and $\frac{l}{r} \ge 15$. These two conditions imply that the opening angle (given by $\tan\delta = \frac{R}{l}$) must be $\delta \le 4^o$. Accordingly, our collimator tube (Fig.4.2) has the following specification: $R$ = 1 cm, $r$ = 0.5 cm, $l$ = 25 cm, $\alpha = 1.146^0$ and $\frac{l}{r} = 50$.

Figure 4.2: Collimator tube mounted on photodiode used as a detector for our pyrheliometer. The inside of this tube is blackened to block circumsolar sky radiation.

**Detector**

Silicon photodiodes are used to convert photonic energy (photons) to electrical current (voltage signal): 13 DAH high-speed mounted silicon PIN photodiode. Its general characteristics such as, spectral response; 350–1100 nm, operating temperature; -10°C to+50°C , photodiode diameter; 0.23mm, make it attractive choice to ensure accurate detection of the intensity of direct solar radiation from visible into the near-infrared. For detail specifications of photodiode used as a detector for our pyrheliometer please visit www.mellesgriot.com

**Filters**

We have color glass filters to obtain a discrete spectral measurement. Measuring their transmittance using a UV source, the filters have wide-bandwidth spectral transmittance nature. The wide spectral range and large number of spectral grids cannot be handled by

the proposed inversion scheme. As a result, we propose effective wavelength and transmittance of a given color filter, is given by weighted sum of spectral transmittance of $i^{th}$ filter, spectral response of the detector and the solar extraterrestrial spectral energy distribution over spectral band:

$$\lambda_{ieff} = \frac{\int \lambda P_i(\lambda)\eta(\lambda)I_o(\lambda)d\lambda}{\int P_i(\lambda)\eta(\lambda)I_o(\lambda)d\lambda} \qquad 4.2.1$$

$$P_{ieff} = \frac{\int P_i(\lambda)\eta(\lambda)I_0(\lambda)d\lambda}{\int \eta(\lambda)I_0(\lambda)d\lambda} \qquad 4.2.2$$

where $\lambda$ - wavelength; $p_i(\lambda)$ - Spectral transmittance of $i^{th}$ filter at wavelength $\lambda$; $\eta(\lambda)$ - Spectral response of the detector at wavelength $\lambda$; and $I_0(\lambda)$ - Solar extraterrestrial spectral energy at wavelength $\lambda$.

Therefore, effective wavelength is the approximate representative of the net effect of all the transmitted spectrum wavelengths and effective transmittance is the approximate representative of the net transmittance of the filter over the whole spectral band covered by the filter. The filters having effective transmittance > 50% for measurement has been used in our study (see Appendix part Table A-1)

**Passive tracker (PST)**

It provided with a sighting arrangement for aiming the pyrheliometer directly at the sun (Fig.4.1). It is manually rotated two axes tracker.

## 4.3 Calibration of the pyrheliometer

To calibrate we use the spectral sensitivity of our detector (Fig.4.3), the solar extraterrestrial spectral energy distribution at mean value of earth-sun distance (Fig. 4.4) and spectral transmittance of each filter.

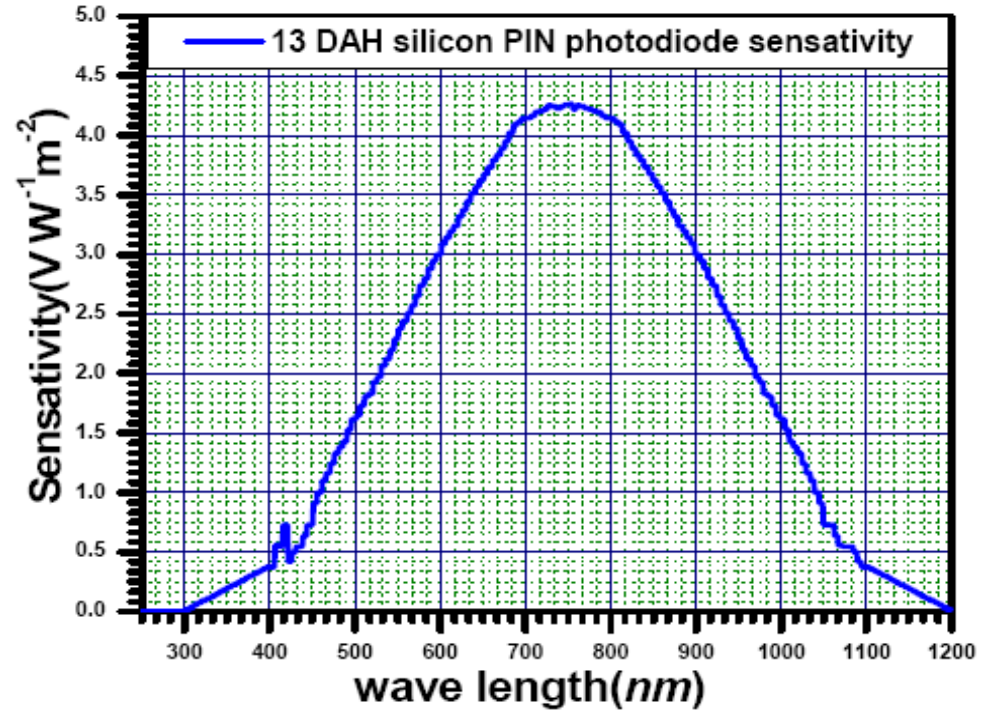


Figure 4.3: Spectral sensitivity of a 13 DAH detector

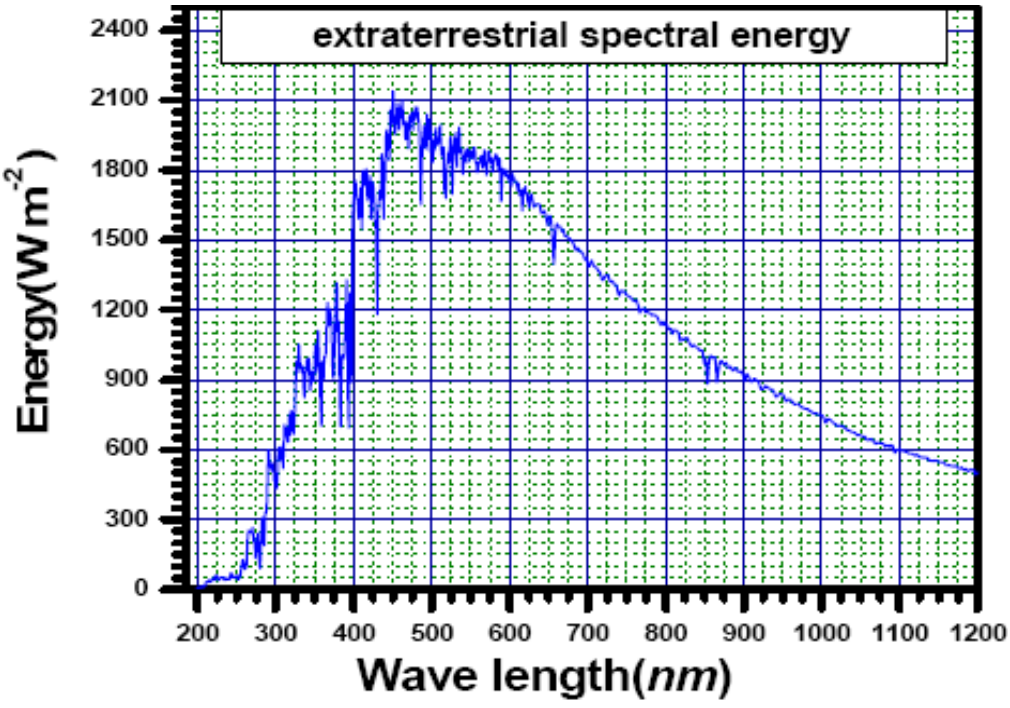


Figure 4.4: Solar extraterrestrial spectral energy distribution (data taken from http://eosweb.larc.nasa.gov/cgi-bin/sse/daily.cgi).

Solar extraterrestrial spectral energy (watts per square meter) to an equivalent mill volt signal at effective wavelength of the $i^{th}$ filter (pyrheliometer spectral calibration constants) is given as

$$V_0(\lambda_{i\,eff}) = \int I_0(\lambda)\eta(\lambda)P_i(\lambda)d\lambda \qquad 4.3.1$$

That is we can derive aerosol optical thickness from surface level solar spectral energy at effective wavelength equivalent mill volt signal directly:

$$V(\lambda_{i\,eff}) = \frac{T(\lambda_{i\,eff})\int I_0(\lambda)\eta(\lambda)P_i(\lambda)d\lambda}{\gamma^2} \qquad 4.3.2$$

where $T(\lambda_{i\,eff})$ effective transmittance or effective transmission coefficient of the Earth's atmosphere at effective wavelength ($\lambda_{i\,eff}$) of the $i^{th}$ filter. Using Eqs. (4.3.1) and (4.3.2), we obtain

$$T(\lambda_{i\,eff}) = \frac{\gamma^2 V(\lambda_{i\,eff})}{V_0(\lambda_{i\,eff})} \qquad 4.3.3$$

Then Eq. (3.3.5) reduce to

$$\tau_A(\lambda_{i\,eff}) = \left[\ln V_0(\lambda_{i\,eff}) - \ln\left(\gamma^2 V(\lambda_{i\,eff})\right) - \tau_M\right] \qquad 4.3.4$$

## 4.4 Measurement and analysis

Measurements are taken when the sky was nearly free from visible clouds, and none were near the line-of- sight to the sun: clear-sky conditions. The reasons for this restriction are three-fold.

Firstly, the effect of aerosols on radiative transfer is best investigated when their effect is isolated, that is when all other contributions are well known. Secondly, sun-photometers cannot easily distinguish cloud optical thickness from aerosol optical thickness. Thirdly, reflections from clouds would affect the amount of diffuse radiation received.

By using a suitable program that takes into account the measurement time of the year and the coordinates of measurement area, which provide the relative angular position of the sun and our manually rotated passive tracker pointing fields of view of the collimator toward the approximate position of the sun. Thus, sequences of spectral measurement are taken using different filter in front of a small aperture through which the direct solar rays enter.

Data obtained with each filter were corrected for background noise by setting the detector output to zero by completely covering the filter before it is exposed to the sun. The procedure is repeated for all the data sets recorded for different solar zenith angles.

Using those recorded data sets at effective wavelength ( $\lambda_{i\,eff}$ ) of the $i^{th}$ filter together with Eqs. (4.3.2) and (4.3.3), effective transmission coefficient of the atmosphere can be calculated.

The value of $T_m\left(\lambda_{eff}\right)$ was estimated from line by line calculations based on direct solar beam spectral transmittance from MODTRAN 3.5 by using tropical model atmosphere, haze free (ideal atmosphere) and other specifications necessary for tropics. Then using Eq. (4.3.4), aerosol optical thickness (AOT = $\tau_A\left(\lambda_{i\,eff}\right)$), for a slant path of the atmosphere can be determined (see Appendix).

# Chapter 5

# Results and discussions

We discuss the retrieval results of optical and microphysical parameters spectral and temporal variations together with modeling the effect of water vapor on hydrophilic aerosols, in different sub sections of this chapter.

## 5.1 Spectral and temporal variations in aerosol optical thickness (AOT)

The spectral AOT are obtained by subtracting the spectral molecular optical thickness from the total spectral optical depth for a slant path of the atmosphere.

The spectral and temporal variations in total column AOT at different effective optical channels of the pyrheliometers observed on a typical clear-sky day (May 21, 2008 and May 23, 2008) are shown in Fig. 5.1 (panel a and b respectively).

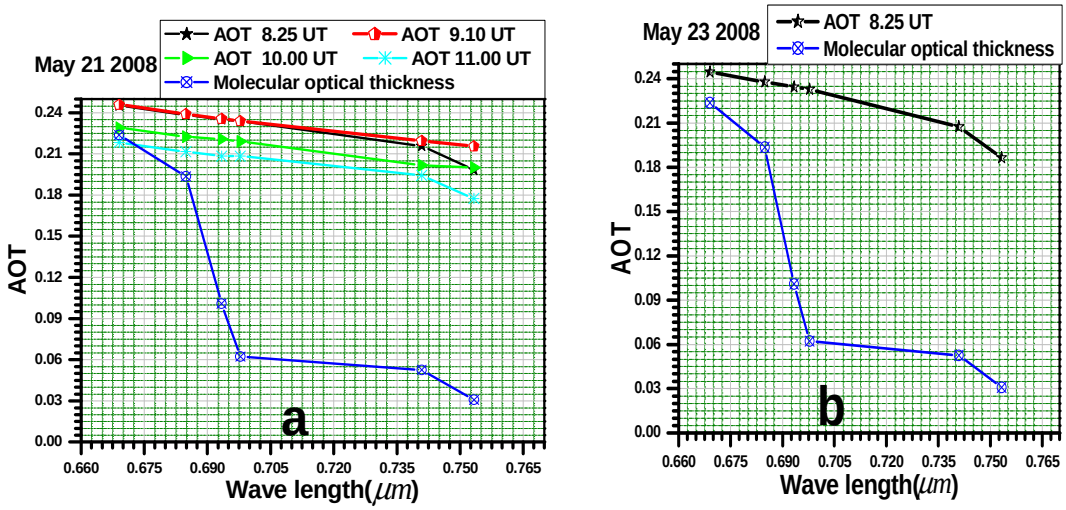


Note: UT – Universal Time

Figure5.1: Spectral and temporal variations in AOT and molecular optical thickness on May 21, 2008, panel (a) and May 23, 2008, panel (b).

The spectral molecular optical thickness in Fig. 5.1 panel (a) and (b) show that the contribution of total gaseous component of the atmosphere to the total spectral attenuation. At $\lambda = 0.669\,\mu m$ the molecular oxygen absorption causes higher molecular optical thickness. Comparison of the optical depth caused by atmospheric aerosols and molecules clearly shows that the main source of radiation attenuation is caused by aerosols.

The panel (a) and (b) the spectral variation of AOT exhibit systematic spectral dependence according to classical Mie theory i.e.

$$Q_s \propto \frac{1}{\lambda^2}$$

In addition, spectral variation of molecular optical depth agrees with Rayligh theory i.e.

$$Q_s(molecular) \propto \frac{1}{\lambda^4}$$

The temporal evolution of normalized spectral average AOT relative to the spectral average AOT in May 21, 2008 at 9.10 UT shows that $\tau_A(at\,9.10UT)$ = $1.018\,\tau_A(at\,8.25UT)$ = 1.075 $\tau_A(at\,10.00UT)$ = 1.142 $\tau_A(at\,11.00UT)$, which indicate that solar radiation attenuation have minimum value during the post-noon and a maximum during the noon. This enhancement mainly depends on concentration of aerosol particles inside the beam path (solar zenith angle) of direct solar radiation pass on and specific condition of the atmosphere at a particular place and time.

The comparison of spectral dependence of AOT during the two days for the same air mass (8.25 UT, $\theta = 31^0$) is shown in Fig.5.2.

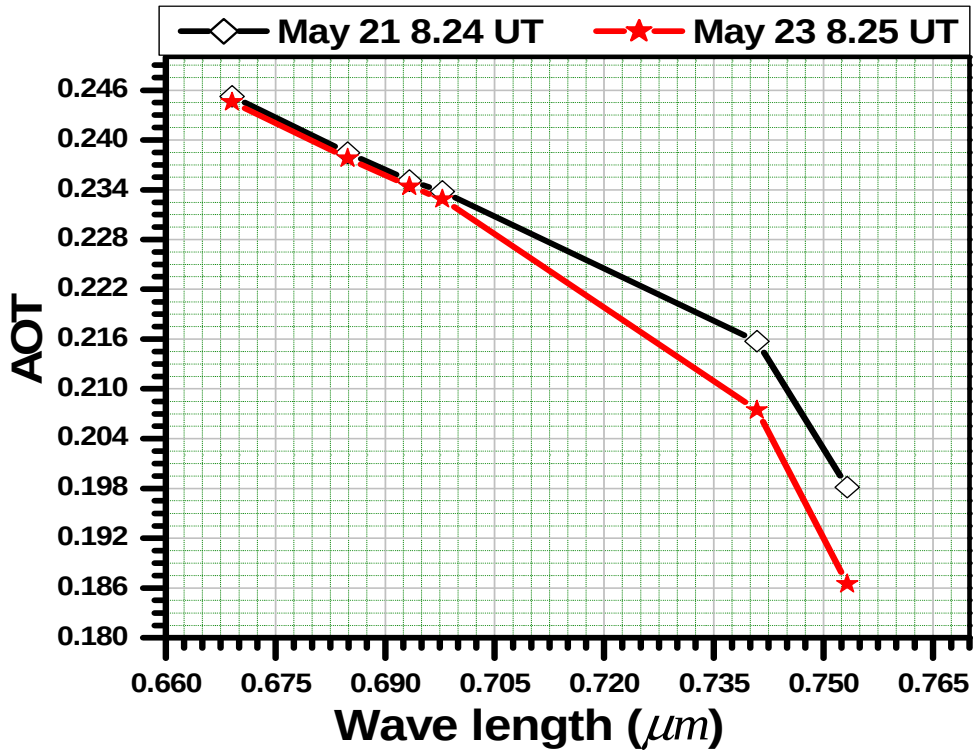


Figure 5.2: The difference of spectral AOD values for the two days (May 21, 2008 and May 23, 2008) at optical mass or air mass factor $m$ = 1.17

The fall in measured AOT from May21, 2008 to May 23, 2008 in Fig. 5.2 needs close inspection. Particularly the deviations in AOT above wave length of 0.7 $\mu m$, needs to be explained. Size selective dynamic process of atmospheric aerosols: smaller particles are comparatively long-lived because fairly buoyant due to Brownian motion and slow growth due to more quick coagulation. While larger particles are comparatively short-lived, for two main reasons: The largest particles have sufficient mass to be affected by gravitational settling: dry deposition (diameter > 5$\mu m$) and act as cloud condensation nuclei (CCN). Nucleation to cloud drops or impaction onto the surface removes larger particles efficiently eventually fall as rain and removed by precipitation: wet deposition.

So the water that increase particle sizes of aerosols depending on their nature, then the gain in size have sufficient mass to be affected by gravitational settling. Also for larger particles, sedimentation becomes an important removal process since the viscous drag is proportional to the particle surface, while the gravitational force scales with the volume.

Therefore, in the radius range of $0.5\,\mu m < r < 2\,\mu m$, wet deposition which is the most efficient removal process when a particles radii increases. As a result, particles density in the radii range above $0.7\,\mu m$ decline causes the fall in AOT.

In order to explain these results in a more detailed way, the physical and chemical nature of aerosols with meteorological parameters such as wind speed, temperature and relative humidity, and a back trajectory analysis must be considered simultaneously.

## 5.2 Retrieved atmospheric aerosols micro physical parameters

In order to retrieve the atmospheric aerosols microphysical parameters: refraction index, size distribution and its geometric shape, we assume that the particles are spherical so that Mie theory could be applied. Aerosol particle size distribution and complex refractive index are fundamentally different parameters. The aerosol optical depth is highly variable in space and time and it is a complex function of refractive index and size distribution. Thus aerosol optical thickness measurements made between six different effective wavelengths ranging between $0.699\,\mu m$ and $0.753\,\mu m$ have been used in the retrieval of aerosol particle size distribution and effective complex refractive index in the total atmospheric column following the inversion scheme suggested by [31-33] (Section 3.4) simultaneously.

### 5.2.1 Effective refractive index

This effective complex index of refraction does not refer to any specific aerosol type but is suitable to quantify the composite radiative properties of all aerosols in an atmospheric column.

In reality, our knowledge of refractive index, however, is uncertain. For aerosols, refractive index is essentially unknown since atmospheric aerosols are mixtures of a variety of aerosol types and chemical compositions (e.g., sulfate, nitrate, ammonium, condensed organic species, elemental or black carbon, and mineral dust). Refractive index generally varies with particle radius due to chemical composition of particles of different sizes; this affects the extinction spectrum, which is used in the retrieval size distribution.

To estimate simultaneously the effective refractive index together with size distribution, the simulated optical thickness is found by using inversion scheme which is stated in (Section 3.4) by varying the complex refractive index of the aerosol particles which is wavelength and size independent and taking the different refractive index in the range between 1.33 and 1.65 for most aerosol types. The retrieval procedure continues until the difference between simulated and measured aerosol optical thicknesses are minimized. Thus, we choose aerosol refractive index having a minimum chi-square ($\chi^2$) error between simulated and measured optical thickness values:

$$\chi^2 = \sum_{i=1}^{n} \left( \tau_{measured}(\lambda_i) - \tau_{simulated}(\lambda_i) \right)^2 \qquad 5.1$$

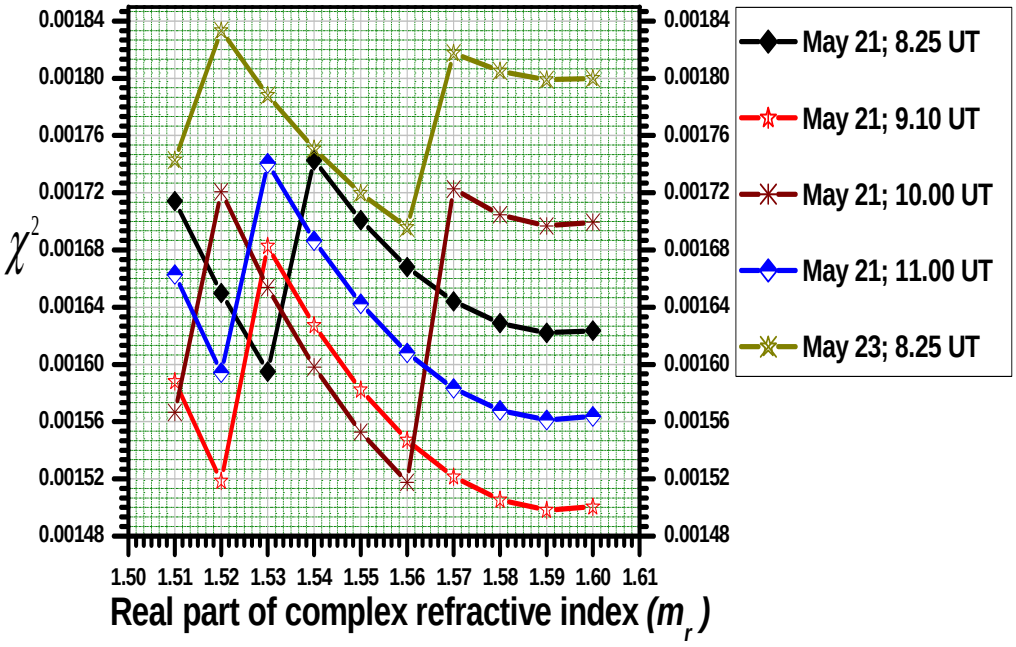


Figure 5.3: Chi-square error verses real part of complex refractive index

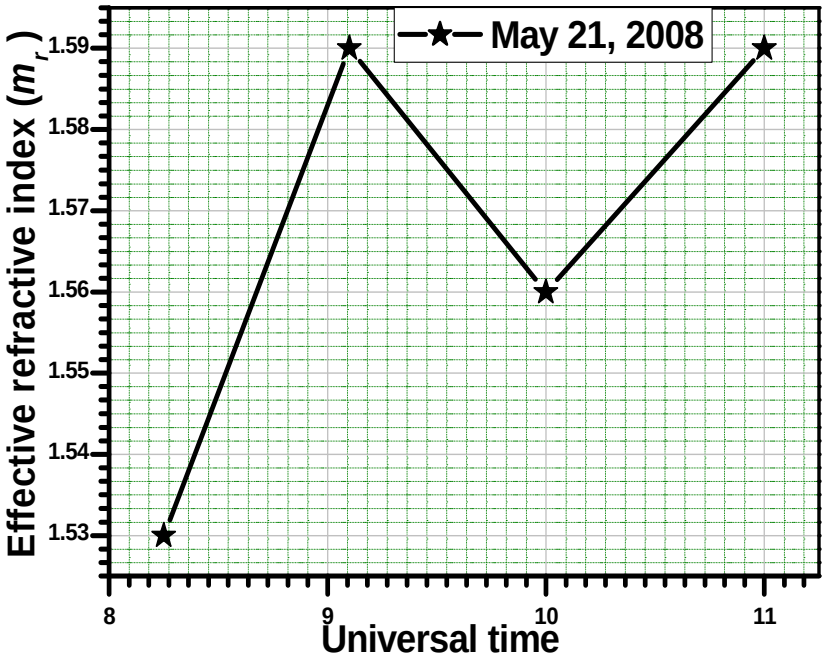


Figure 5.4 Temporal variation of real part of aerosol effective refractive index on May 21, 2008

Imaginary part of aerosol effective refractive index determined on the ground level for different periods on May 21, 2008 is almost constant ~ 0.0005. Aerosol effective refractive index determined on the ground level for May 23, 2008 ~1.56+ $i$ 5x10$^{-4}$.

The reason for the temporal variation of effective refractive index is mainly related to meteorological parameters such as wind speed, temperature and relative humidity together with the physical and chemical nature of aerosols. The main metrological parameter that causes this variation is water vapor [36]. By modeling the effect of water vapor, the temporal variation will be further investigated in the next section.

## 5.2.2 Modeling the effect of water vapor

To model the effect of water vapor on hydrophilic aerosols, for describing aerosol growth and optical effect, we used mixing rules for refractive indices. The appropriate mixing rule for the inclusion of an insoluble core in a liquid host medium is the Maxwell-Garnet mixing rule. However, it requires the explicit choice of a host and an inclusion medium.

A more accurate approximation for effective refractive indices can be obtained from mixing rules derived from effective medium approaches, quantifying the macroscopic radiative properties as an average over the microscopic arrangement of the components [37].

A general formulation for mixing rules of *n* components can be expressed as [36]:

$$\frac{\varepsilon_{eff} - \varepsilon_0}{\varepsilon_{eff} + 2\varepsilon_0} = \sum_{k=1}^{n} f_k \frac{\varepsilon_k - \varepsilon_0}{\varepsilon_k + 2\varepsilon_0} \qquad 5.2$$

where $\varepsilon_{eff}$ is the complex effective dielectric constant of the mixture, $\varepsilon_0$ is the complex dielectric constant of the host medium, and $\varepsilon_k$ and $f_k$ are the complex dielectric constant and volume fraction of component *k*, respectively. Complex refractive index is given by $m_i = \sqrt{\varepsilon_i}$. Choosing the urban aerosol which is a mixture of several chemical components as a single inclusion medium having a net complex refractive index whose real part is 1.6 in a non hydrated state i.e. $\varepsilon_k = \varepsilon_{net} = 2.56$ and the water droplet as host medium i.e. using the refractive index of pure water $\varepsilon_0 = 1.7689$ as an inclusion medium, then Eq. (5.2) can be reduces to

$$f_k = 7.708\left(\frac{\varepsilon_{eff} - 1.7689}{\varepsilon_{eff} + 3.5378}\right) \qquad 5.3$$

Using the aerosol effective refractive index determined on the ground level for different periods, volume fraction of dry urban aerosol ( $f_k$ ) form wet urban aerosol can be found. This can be done assuming the urban aerosol have a spherical shape in both dry and wet state as $\left(f_k\right)^{\frac{-1}{3}} = \frac{r_{w\,eff}}{r_{d\,eff}}$, where $r_{d\,eff}$ and $r_{w\,eff}$ are effective radius of urban aerosol in a

and wet conditions respectively.

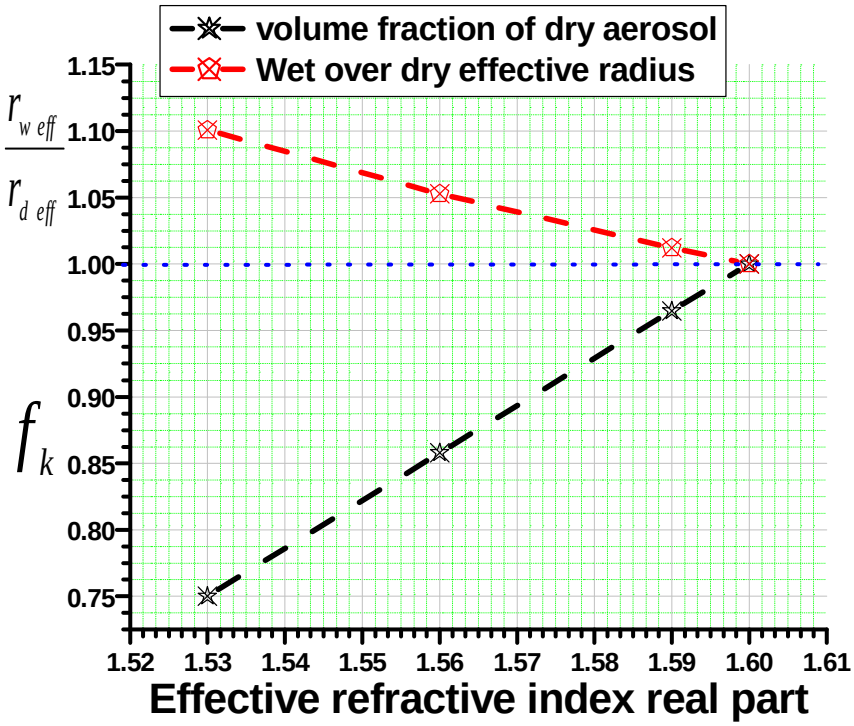


Fig 5.5: Volume fraction of dry aerosol and effective radius ratio of aerosol in a wet condition over dry conditions verses effective refractive index.

Using this assumption it is clear that $\frac{r_{w\,eff}}{r_{d\,eff}}$ and effective refractive index show opposite variation as the water uptake by the particles gets more and more important. With increasing relative humidity, particles may accrete water vapor by deliquescence and further by hygroscopic growth. With decreasing relative humidity, water is lost and ultimately particles may effloresce to the dry state. The uptake of water increases particle size, there by affecting the particle optical properties. Apart from the change in size, hygroscopic aerosols experience a change in their refractive index as RH increases. Generally, as the water uptake by the particles gets more and more important, the real and imaginary parts of their refractive index tend to decrease.

However, the scattering is a complex function of refractive index and particle size, both effects need to be taken into account (already discussed in section; Eq. 2.4.24). In fact,

variations in refractive index as RH increases are not large enough to counteract the variation of the particle's cross-section due to size increase ($r^2$ dependence). Therefore, the size dependence dominates, leading to an increase in scattering efficiency as RH increases.

We also used the Aerosol Chemistry Data analysis result [36, 37, and 38]. The mean aerosol refractive index assumed to be derived from the volume-weighted molar refractivity. Similarly, the mean aerosol density was obtained from the volume-weighted component densities. It was found that, on average, the real part of the refractive index of dust aerosols could be expressed by the relation $m_{eff.} = 1.78(1 - RH)^{0.07}$, where RH is the relative humidity (expressed as a fraction, not a percentage). This result is applicable for humidities up to around 95%.

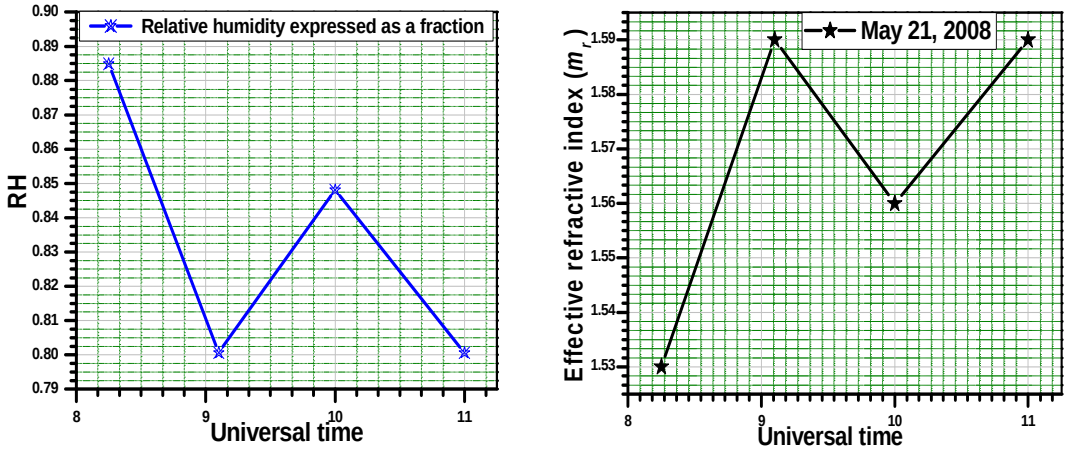


Figure 5.6: Left panel: Relative humidity at surface; Right panel: real part of aerosol effective refractive index, temporal variations.

## 5.3 Columnar aerosol size distribution (ASD)

Aerosol particles are not monodisperse but rather appear continuous size distributions: size distributions describe the number of particles observed in a certain radius size ranges and is a function of position. However, radiances measured at the ground are influenced by the whole atmospheric column and are not expected to be strongly dependent on the vertical distribution of aerosol. Consequently, most ground-based retrievals characterize the optical properties of the aerosol in the total atmospheric column (columnar aerosol).

Therefore, the single scattering properties of each particle size must be appropriately weighted and combined into the net or effective single scattering properties of the entire size distribution.

Practical algorithms are often designed to retrieve the size distribution of surface area of aerosol particles since light scattering of a small single particle is a function of particle surface area rather than number concentration.

Particle size distribution is modeled by power-law size distribution in our study. We have chosen aerosol refractive index having a minimum chi-square error between simulated and measured optical thickness values to estimate simultaneously the effective refractive index.

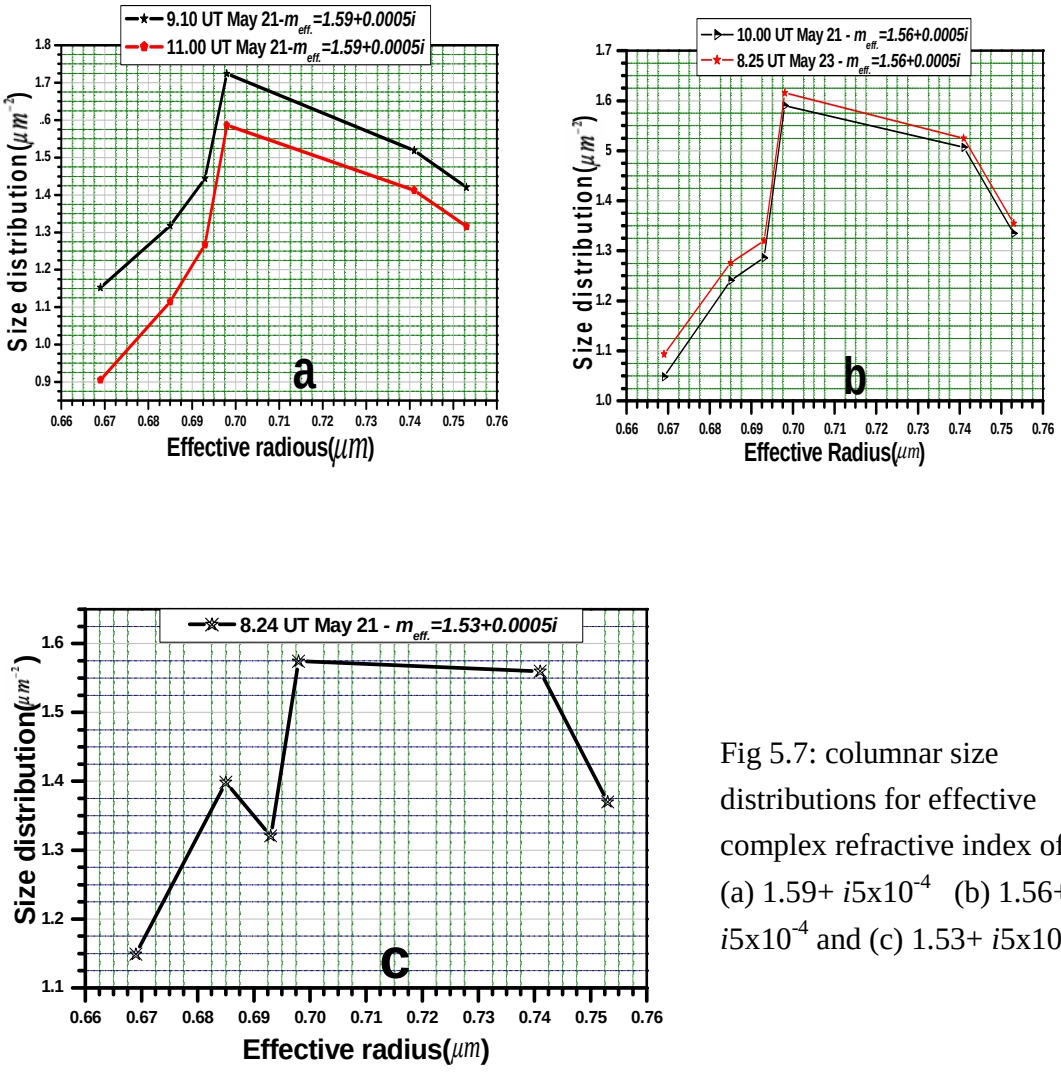


Fig 5.7: columnar size distributions for effective complex refractive index of (a) 1.59+ $i$5x10$^{-4}$ (b) 1.56+ $i$5x10$^{-4}$ and (c) 1.53+ $i$5x10$^{-4}$

The above results indicate that power-law size distribution deviates from all retrieved size distributions. So far, our discussion deals with corresponding to minimum chi-square ($\chi^2$) which describe the sum of differences between simulated and measured aerosol optical thicknesses as defined in Eq. (5.1) columnar aerosol size distributions. The retrieved size distributions maintain similar shape for the same values of effective complex refractive index over the entire effective radii of aerosols. Change in effective complex refractive index, which depends on chemical nature of aerosols and specific atmospheric conditions, produce changes in the magnitude of the retrieved size function (f(r)) and hence the retrieved size distribution. This indicates that the concentration of aerosols in the atmosphere not only depends on their physical properties but also depends on their chemical properties.

Within range of effective radius used in this thesis (0.669 $\mu m$ - 0.753 $\mu m$) effective modal radius of the aerosol particle can be determined by using a modal- function generally spanning from positive to negative value when atmospheric particles decay in modal concentration.

$$M_k = \frac{ASD_{i+1} - ASD_i}{r_{eff.\,i+1} - r_{eff.\,i}},$$

where $r_{eff.\,i}$, and $ASD_i$ are the $i^{th}$ effective radius of the entire size distribution and its corresponding columnar size distribution respectively.

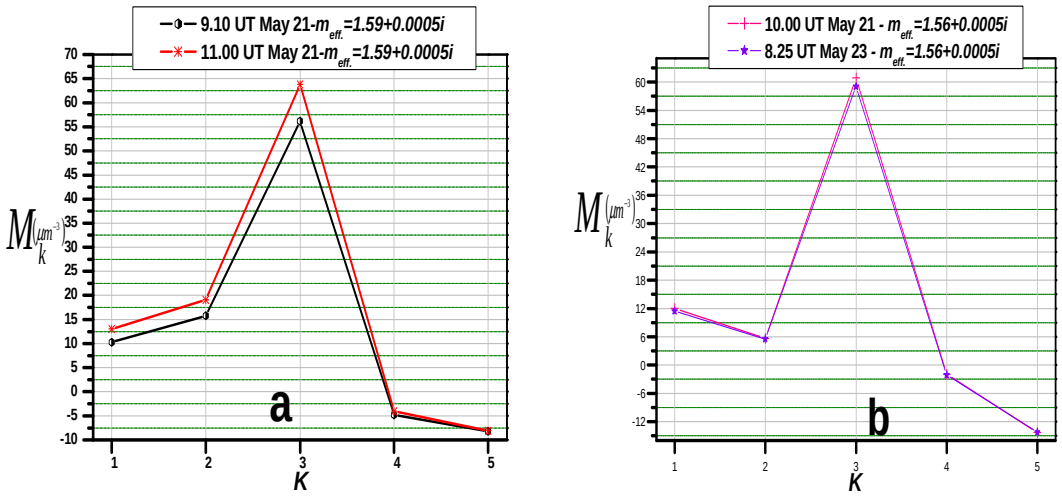

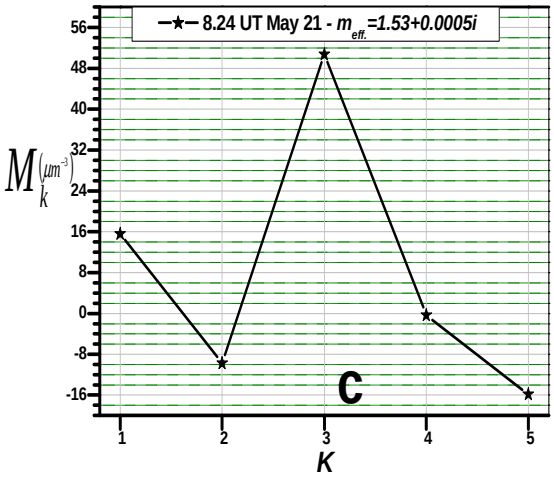


Figure 5.8: Rate of change of columnar size distribution for effective complex refractive index of (a) 1.59+ $i$5x10$^{-4}$

(b) 1.56+ $i$5x10$^{-4}$

(c) 1.53+ $i$5x10$^{-4}$

Panels (a) in Fig. 5.7 and Fig 5.8 show monomodal size distribution with mode effective radius of 0.698 $\mu m$ . Particles around mode radius have maximum concentration at 9.10 UT and 11.00 UT on May 21. The average columnar size distribution over effective radius at 9.10 UT is 1.139 times the average columnar size distribution at 11.00 UT on May 21. This relationship is also valid for spectral average AOT i.e. AOT at 9.10 UT is 1.142 times that of at 11.00 UT. This indicate that the optical properties of aerosol such as scattering phase function, single-scattering albedo, and the spectral variation of AOT is directly depends on the there size distribution. This can be even more evident if we normalize both average retrieved columnar size distribution and the spectral average of measured optical thickness values to their corresponding average values over the particle radii and spectral range at 9.10 UT on May 21.

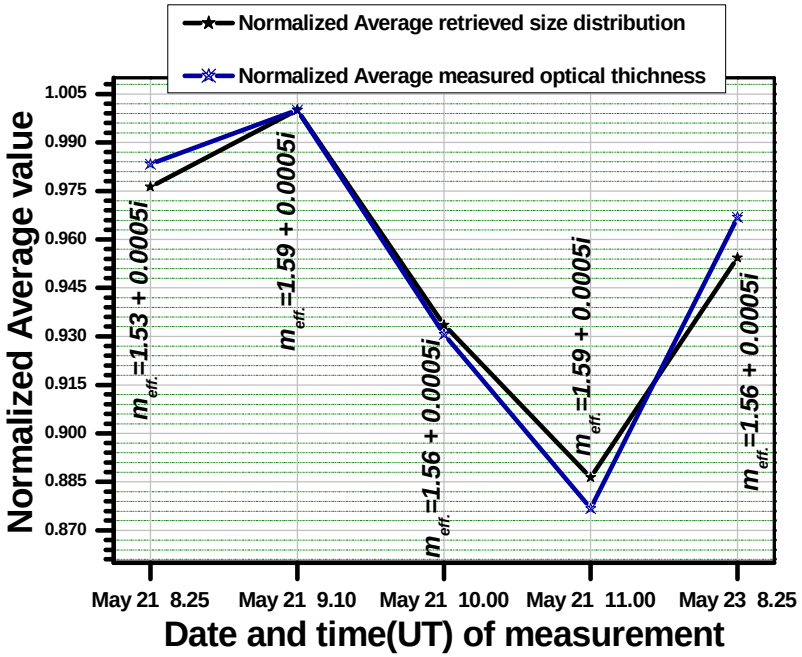


Figure 5.9: Normalized values of measured spectral average optical thickness and average retrieved columnar size distribution with corresponding temporal values of effective complex refractive index.

Both measured spectral average optical thickness and average retrieved columnar size distribution show the same variation with time as clearly depicted in Fig. 5.9. The temporal variation shows peak values for both average optical thickness and retrieved size distribution at noon. The main cause of temporal variation including the peak values at noon depends on the aerosol production and removal rates along with specific atmospheric conditions.

The decrease in optical thickness at 8.25 UT (air mass factor $m(\theta = 31^0)$= 1.17) from May 21, 2008 to May 23, 2008 as given in Fig. 5.2 can not be explained by a corresponding increase in real parts of refractive index. However, decrease in optical thickness over this period could be linked to the decline in aerosol size distribution, which is evident in Fig. 5.9. This is also in support of our previous claim in section 5.1 that the difference in aerosol optical thickness between the two days is caused by the removal of particles due to gravitational settling and wet deposition, which are the most efficient removal process for coarse mode aerosols.

Based on mixing rules given in section 5.2.2, we have assumed effective refractive index of $m_{eff}$ =1.6+ $i$5x10$^{-4}$ to calculate effective radius in a dry condition from our experimental values of columnar urban aerosols having 0.685 $\mu m$ effective radius and effective refractive index $m_{eff}$ =1.53+ $i$5x10$^{-4}$ in a wet condition. As a result, effective radius of 0.622 $\mu m$ is obtained in a dry condition.

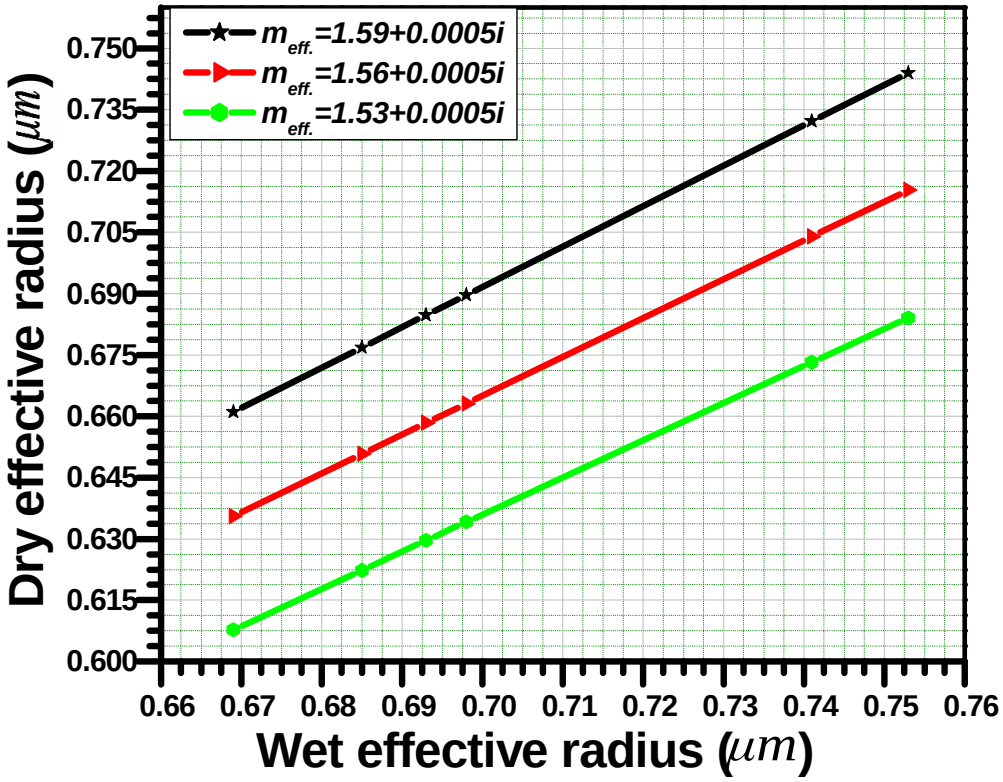


Figure 5.10 Effective radius of urban aerosol in a dry condition determined using mixing rules for each retrieved effective refractive index.

Thus, effective radius of urban aerosol in a wet condition as well as in a dry condition indicates that the retrieved aerosols are coarse mode.

The coarse mode particles are the primary particles that are directly injected into the atmosphere from sea-salt particles over the ocean, fine sand particles and biogenic dust

from the land. Therefore, our experiment reveals that from long time measurement along with meteorological parameters one can estimate the main sources of our city aerosols.

## 5.4 Optical parameters of aerosols

In order to determine the optical properties related with the interaction between the atmospheric aerosols and solar radiation it is necessary to know parameters such as refraction index, size distribution and its geometric shape. However if we assume that the particles are spherical, Mie theory could be applied in conjugation with inversion model to obtain aerosol size distribution and effective refractive index from solar radiation measurements. Thus, we can compute aerosol radiative properties such as single-scattering albedo (SSA), phase function**.** In practice the phase function is parameterized with asymmetry factor (g) and hemispheric backscattered fraction ($\beta$): a fraction of the scattered intensity that is redirected into the backward hemisphere of the particle, which depends on the solar zenith angle as well as the size distribution and chemical composition of the particles. Those relevant aerosol optical parameters serve as input to models dealing with aerosols effects in the energy budget, radiative forcing and for the study of aerosols semi-indirect and indirect climatic effects.

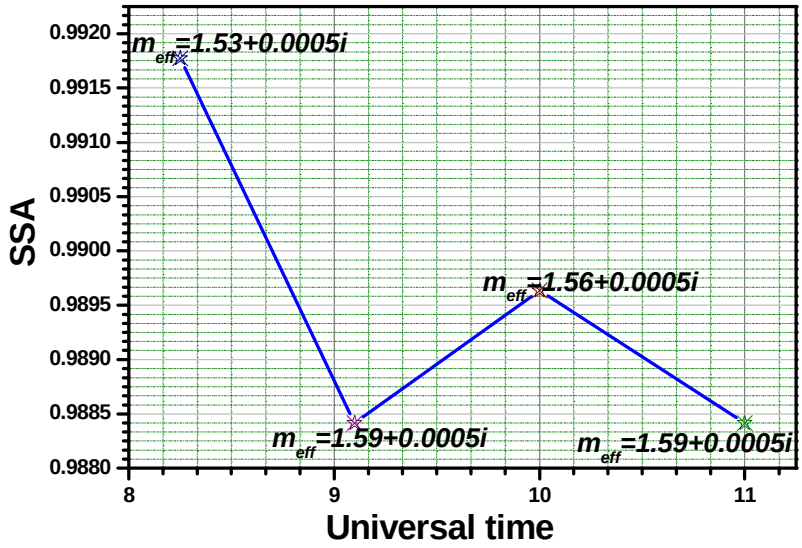


Figure 5.11: Temporal variation of single-scattering albedo and the corresponding effective refractive index calculated from the inversion of solar radiation measurements.

The aerosol single-scattering albedo describes the relative contributions of scattering and absorption to the total light extinction. Fig. 5.11 indicates that, hydrophilic aerosols become larger and more scattered with increasing relative humidity of air.

The direct radiative effect of aerosols is also very sensitive to the single scattering albedo. For example, a change in SSA from 0.9 to 0.8 can often change the sign of the direct effect, depending on the albedo of the underlying surface and the altitude of the aerosols [39].

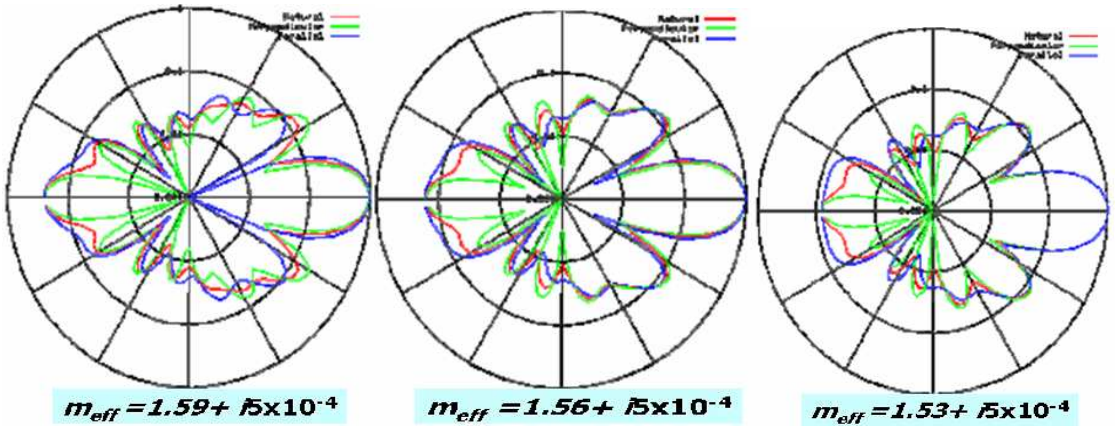


Figure 5.12: Phase function (angular distributions of scattered radiation) for the corresponding effective refractive index indicated in the legend.

Radiative transfer models commonly require one of two integral properties of the angular distribution of scattered light (phase function): the asymmetry factor ( $g$ ) or hemispheric backscattered fraction ( $\beta$ ).

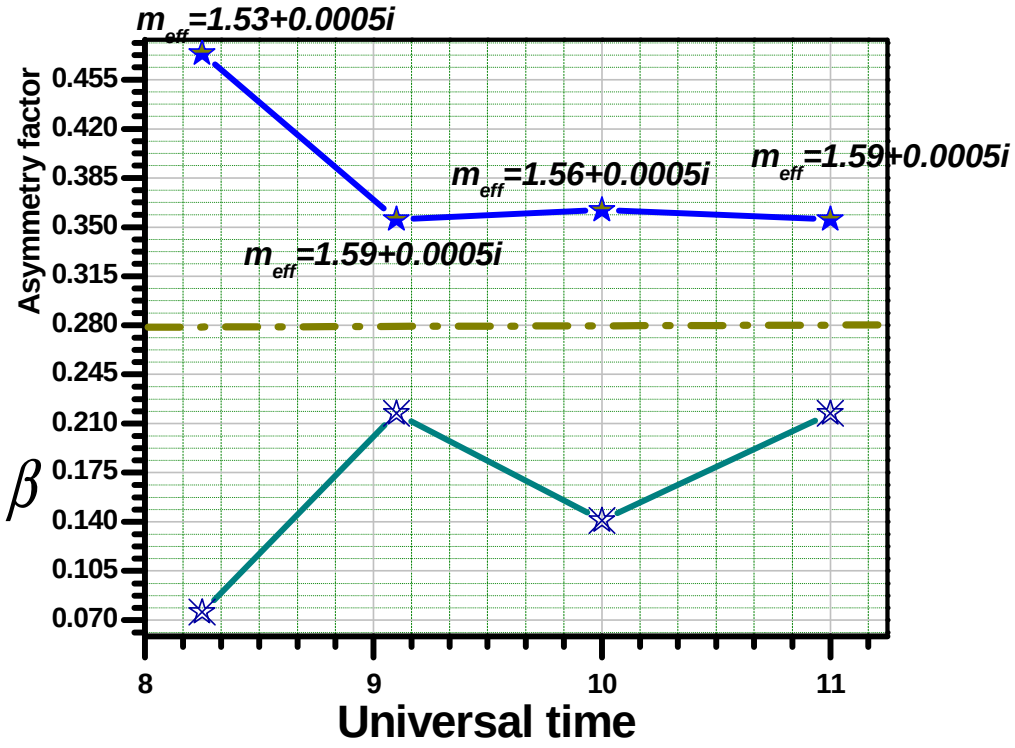


Figure 5.13: Asymmetry factor ( $g$ ) and hemispheric backscattered fraction ( $\beta$ ) for a given aerosol size distribution having effective refractive index shown in the legend.

Fig. 5.12 and 5.13 have revealed excellent correlation with the effect of water vapor, such that the larger the particle size, the more the scattering in the forward hemisphere (i.e., larger $g$ and smaller $\beta$).

Therefore, under dry conditions dust component dominated the atmosphere having a much-contrasted radiative effect depending upon the brightness of the underlying surface. Over bare surfaces with a large surface albedo (>0.30) the dust aerosols will always warm the atmospheric column. Even though under dry conditions dust aerosols hemispheric backscattered ratio reach 21 .73% (see Fig. 5.13) the forward hemisphere scattered component of radiation gets more reflectance due to bare surfaces with a large surface albedo. Thus this component also get backscattered to ward the surface with the same value of hemispheric backscattered ratio than due to the absorption of this radiation by greenhouse gases atmospheric column.

Dark surfaces such as oceans and deciduous forests, where surface albedo is less than 0.15, the effect of dry dust aerosols is to cool the atmospheric column. That is, less amount of radiation under goes hemispheric backscattering to ward the surface than hemispheric backscattering to ward the space.

Over surface albedos in the intermediate range, 0.15<A<0.30, the sign of the forcing depends mainly on four factors, the size distribution, the dust composition, the wavelength of incident light, and the ambient relative humidity (RH). These all determine the single scattering albedo of the particles.

## 5.5 Validation

Validation is the process of checking if something satisfies a certain criterion or validation refers to establishing documented evidence that a process or system when operated within established parameters can perform effectively and reproducibly to produce correct or suited result for its intended use. Validation is important because it disallows data that cannot possibly be either true or real to be entered into a database or computer system.

Consequently, comparisons of spectral average total column AOT determined from pyrheliometer observation of atmospheric spectral transmission and computed spectral average effective SSA at $\left(\lambda_{i\,eff}\,(average)=706nm\right)$, on a typical clear-sky days (May 21, 2008 and May 23, 2008) and monthly average satellite data and model retrieval result from AEROCOM global climatology of AOT and SSA (May) at $\left(\lambda=550nm\right)$:

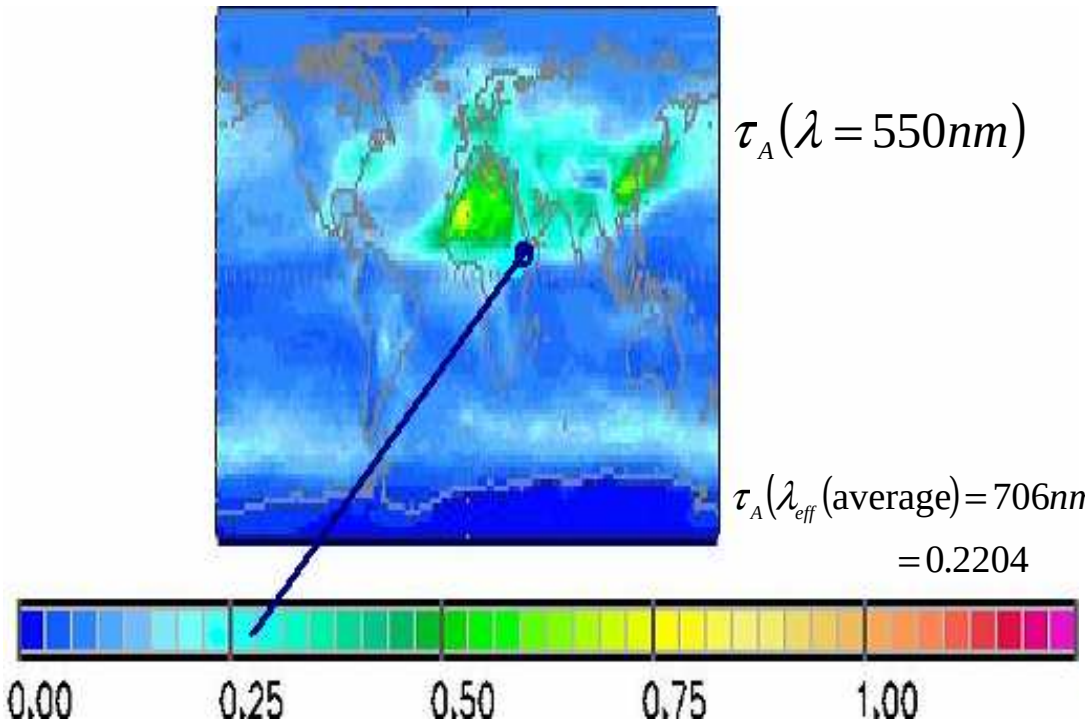


Figure 5.14: Comparisons of spectral average total column AOT and AEROCOM (taken from http://nansen. ipsl. jussieu. AEROCOM)

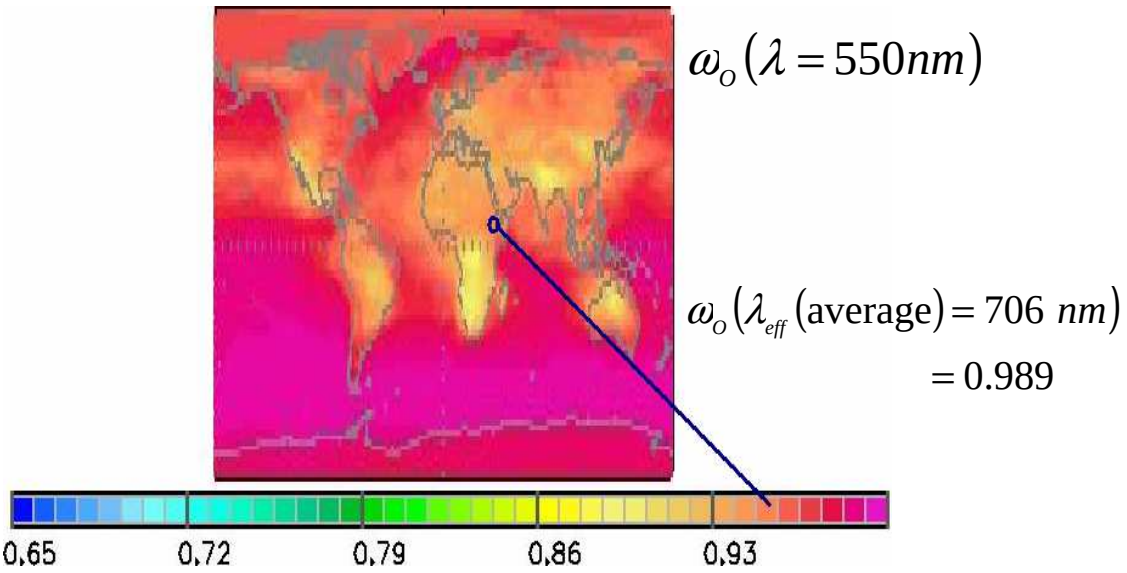


Figure 5.15: Computed spectral average effective SSA and AEROCOM (taken from http://nansen. ipsl. jussieu. AEROCOM)

Since the spectral variation of AOT from the Mie theory i.e. $Q_S \alpha \frac{1}{\lambda^2}$ , that is AOT determined from pyrheliometer observations and SSA determined from inverse modeling of AOT (size distribution and effective refractive index) associated with Mie theory shows a nice agreement with AEROCOM global climatology of monthly average (May) results.

Aerosols in urban areas are however complex and are generally a mixture of several chemical components including organic carbon, soot, water-soluble, dust and sea salt. Depending on the chemical compositions of aerosols, the complex refractive index is highly variable [36]. Several models and most traditional studies based on bulk chemical analyses suggest that the real part of the complex refractive index of urban atmosphere having dominant dust aerosols is $1.57 \pm 0.04$ and SSA exceeds 0.9 in the visible and near infrared spectral regions [18-20, 39 and 40]. Our study shows that retrieved effective refractive index, real part varies in both days from 1.53 up to 1.59 or the daily mean of 1.5675 and 0.989 SSA. Thus, we can deduce that dust is by far the dominant aerosol component in Addis Ababa location.

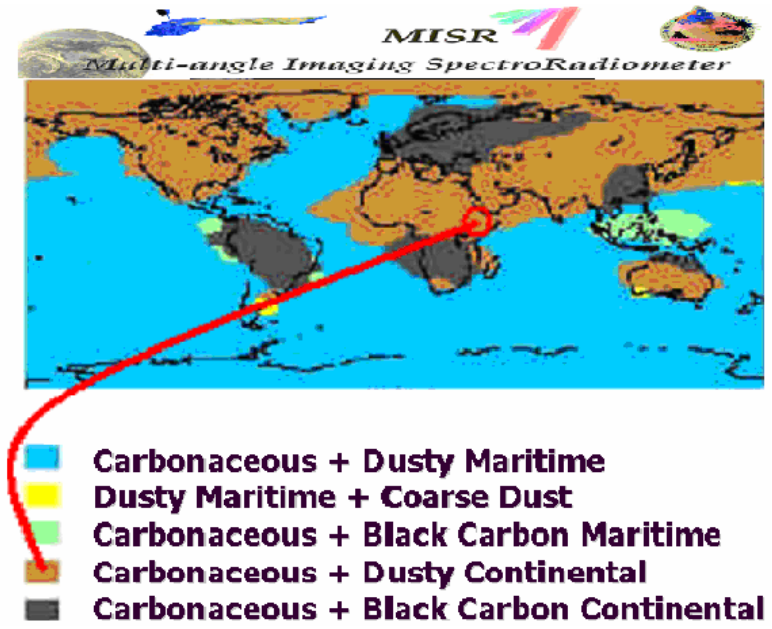


Accordingly, the analysis of aggregate of five-aerosol transport model using MISR remote sensing of tropospheric aerosols data sets (taken from http://eosweb.larc.nasa.gov), it figure out Addis Ababa as carbonaceous + dusty continental. That is, pleasant agreement with our realization.

## 5.6 Conclusions

In this thesis part, we retrieve column integrated effective optical and microphysical parameters of aerosol over Addis Ababa (specifically around ARAT KILLO: + 9° 1′ 48″ N, +38° 44′ 24″ E and elevation 2,355 m (7,726 ft)). Atmospheric aerosols as well as their spectral and temporal variations together with modeling the effect of water vapor on hydrophilic aerosols, optical and microphysical properties are discussed. The Measurements were performed based on the concepts of ground based passive remote sensing method typically direct component of solar radiation; it is carried out using homemade pyrheliometer, which has effective optical channels in order to make discrete spectral measurement. The data collections are performed for clear-sky days on May 21, 2008 and May 23, 2008. The results of the analysis of optical and microphysical parameters of atmospheric aerosols indicate the following points.

Spectral dependence of molecular optical depth and AOT indicate that, higher values at smaller wavelengths and vice-versa as expected from Mie and Rayleigh elastic scattering process.

Temporal variations in AOT in May 21, 2008 resulted mainly from specific condition of the atmosphere at a particular place and time. This implies aerosols have a wide dynamic range of composition and shape, depending on their sources and atmospheric processes.

The fall in measured AOT from May 21, 2008 to May 23, 2008, particularly the deviations in AOT above wavelength of $0.7\,\mu m$, leads us to notice removal processes of particles are more efficient when the gain in size have sufficient mass to be affected by gravitational settling. Also for larger particles, sedimentation becomes an important removal process since the viscous drag is proportional to the particle surface, while the gravitational force scales with the volume and smaller particles are comparatively long-lived.

We used inversion technique to retrieve the particle size distributions from measured extinction data (aerosol optical depth) at six different wavelengths in the range between $0.699\,\mu m$ and $0.753\,\mu m$. During the inversions, we assumed the aerosol particles are spherical and the complex indexes of refraction of the particles are independent of wavelength and particle radius. However, by taking the different complex refractive index of the aerosols we choose aerosol refractive index having a minimum chi-square

error between simulated and measured optical thickness values, this enable us to simultaneously estimate of effective refractive index and size distribution.

The effective refractive index calculated in the framework of Mie theory shows temporal variation related to the effect of water vapor and aerosol Chemistry Data analysis. A good reasonable agreement implies the hygroscopic growth is facilitated by chemical alterations of the dust aerosol surface induced by industrial emissions. As a result, the real and imaginary part of their refractive index tends to decrease. Tropospheric dust aerosol may lose its non-spherical character by condensation of water vapor from the surrounding air on the particle surface. Thus stratospheric dust aerosol from volcanic eruptions is likely to retain its irregularity for a long time due to the low stratospheric water vapor abundance.

Several models and those traditional studies based on bulk chemical analyses suggest that the atmospheric aerosols, which are dominant in Addis Ababa location, are dust aerosols.

Temporal variation of columnar size distribution related to modeling the effect of water vapor suggest that the size distribution varies considerably, with relative humidity, as well as, the atmospheric particle size distribution shows similarity for the equivalent effective refractive index. This implies that, within this narrow range, the atmospheric aerosols have chemically distinct compositions due to their different sources.

An aerosol size distribution shows strong source strength of atmospheric particles around $0.698\,\mu m$, effective radius. The source strength depends critically on the wind speed and the turbulent state of the boundary layer, atmospheric processes, as well as on local soil properties, topography, hydrology etc.

The observations of decline in size distributions of particles mostly above $0.698\,\mu m$ effective radius; implies size selective process. This reflects adhesion forces between particle and the ground. Particles require a certain mass in order to cross the laminar layer of air and thus enter the turbulent regime where efficient vertical transport is possible and dry deposition (primarily sedimentation). These all together are the main removal process when particle's size increases.

We have also computed wavelength independent i.e. effective aerosol radiative properties such as single-scattering albedo (SSA), phase function**,** the effect of water vapor.

Hydrophilic aerosols become larger and more scattering in the forward hemisphere (i.e., larger $g$ and smaller $\beta$) with increasing relative humidity of air.

The computed single scattering albedo, which exceeds 0.9, is indicative that dust is by far the dominant aerosol component. Under dry conditions atmosphere is dominated by the dust aerosols having a much-contrasted radiative effect depending upon the surface albedo (A): A>0.30 will warm the atmospheric column and A<0.15 will cools the atmospheric column.

All the above discussions clearly express difficulties in quantifying aerosol influences arise from the heterogeneity of aerosol loading and properties: spatial, temporal, size, and composition. This multidimensional heterogeneity makes the characterization of aerosols and quantification of their influences on climate and climate change extremely challenging.

The main source of errors such as, solar zenith angle (air mass) precession, proposed effective wavelength and transmittance of a given color filter, calibration source data's and other introduce uncertainties in the retrieval results of optical and microphysical parameters spectral and temporal variations. We further planned to take a long-term measurement and to validate our result in comparison with satellite based aerosol optical thickness measurements and model data's.

Because of non-sphericity of aerosol particles, development of retrieval algorithms based on T-matrix theory, for forward modeling should be pursued.

# Appendix

Measurements are taken when the sky was nearly free from visible clouds, and none were near the line-of- sight to the sun: clear-sky conditions.

The voltage $V_0(\lambda_{i\,eff})$, the extraterrestrial constant (calibration constant), is determined for the instrument to convert the solar extraterrestrial spectral energy distribution (watts per square meter) to an equivalent mill volt signal. It is the voltage our pyrheliometer would see if it were pointed at the sun just outside the earth's atmosphere when the earth is one astronomical unit (AU) from the sun.

This calibration value depends primarily on the wavelength at which the radiation-sensing element of pyrheliometer detects light and on the distance between Earth and the sun. This distance varies slightly because Earth follows a slightly elliptical, rather than a circular, path around the sun. Thus, $\gamma = \frac{R}{R_0}$ is the ratio of the earth-sun distance to its mean value, in units of AU, used to correct the constant $V_0(\lambda_{i\,eff})$. Using the values of 137 and 139 Julian day ( $J$ ) i.e. dates on which a measurements are made, in Eq. (3.2.3), $\gamma$ = 0.985. Using this value the corrected and the mean values of spectral extraterrestrial constant used for our analysis and effective transmittance and its corresponding effective wavelength of the filters used for measurements are given below

**Table A-1**

| $i$ | $\lambda_{i\,eff}(\mu m)$ | $P_{i\,eff}(\%)$ | $V_0(\lambda_{i\,eff})$ | $\frac{V_0(\lambda_{i\,eff})}{\gamma^2}$ |
|---|---|---|---|---|
| 1 | 0.669 | 0.715537 | 15.02622 | 15.47499 |
| 2 | 0.685 | 0.631168 | 13.25447 | 13.65033 |
| 3 | 0.693 | 0.670855 | 13.72794 | 14.13794 |
| 4 | 0.698 | 0.799854 | 16.8891 | 17.39351 |
| 5 | 0.741 | 0.701475 | 14.73091 | 15.17087 |
| 6 | 0.753 | 0.595052 | 12.49604 | 12.86925 |

$V(\lambda_{i\,eff})$ is the voltage record when we point our pyrheliometer at the sun, minus the dark voltage. The air mass *m* (also called atmospheric mass) for a plane-parallel atmosphere, it is determined by Eq. (3.2.4). These values of $V(\lambda_{i\,eff})$ for May 21, 2008, and May 23, 2008, different measurement local time (LT) with corresponding air mass factor are given in Table A-2

**Table A-2**

| **Measured $V(\lambda_{i\,eff})$(mv)** | | | | | | |
|---|---|---|---|---|---|---|
| $i$ | $\lambda_{i\,eff}\,(\mu m)$ | **May21, 2008; 5.24(LT), $m(\theta)$= 1.167** | **May21, 2008; 6.10(LT), $m(\theta)$= 1.005** | **May21, 2008; 7.00(LT), $m(\theta)$= 1.015** | **May21, 2008; 8.00(LT), $m(\theta)$= 1.305** | **May23, 2008; 5.25(LT), $m(\theta)$= 1.167** |
| 1 | 0.669 | 9.681471 | 9.67569 | 9.838755 | 9.946538 | 9.687942 |
| 2 | 0.685 | 8.861616 | 8.85636 | 9.004606 | 9.102593 | 8.867498 |
| 3 | 0.693 | 10.10415 | 10.09818 | 10.2495 | 10.37697 | 10.11084 |
| 4 | 0.698 | 12.93672 | 12.9341 | 13.12799 | 13.27037 | 12.94858 |
| 5 | 0.741 | 11.60089 | 11.55843 | 11.76428 | 11.85217 | 11.69754 |
| 6 | 0.753 | 10.23526 | 10.05745 | 10.21677 | 10.44883 | 10.35519 |

Using those recorded data sets at effective wavelength ( $\lambda_{i\,eff}$ ) of the $i^{th}$ filter together with Eqs. (4.3.2) and (4.3.3), the value of effective transmission coefficients of the total atmosphere ($T(\lambda_{i\,eff})$) can be calculated. The corresponding contribution of effective transmission coefficient of the molecular atmospheric component ($T_m(\lambda_{eff})$) values estimated from MODTRAN 3.5 by using all necessary specifications for tropical model atmosphere. The values of $T(\lambda_{i\,eff})$ and $T_m(\lambda_{eff})$, as well as there logarithm which gives total spectral optical depth for a slant path of the atmosphere ($\tau_{atm}(\lambda_{i\,eff})$) and molecular optical depth ( $\tau_M$ ) of the atmosphere are given in Table A-3 and A-4 respectively.

**Table A-3**

| Atmospheric effective transmission coefficient ($T(\lambda_{i\,eff})$) | | | | | | | |
|---|---|---|---|---|---|---|---|
| $i$ | $\lambda_{i\,eff}(\mu m)$ | **May21, 2008; 5.24(LT), $m(\theta)$= 1.167** | **May21, 2008; 6.10(LT), $m(\theta)$= 1.005** | **May21, 2008; 7.00(LT), $m(\theta)$= 1.015** | **May21, 2008; 8.00(LT), $m(\theta)$= 1.305** | **May23, 2008; 5.25(LT), $m(\theta)$= 1.167** | **Molecular transmiss-ion coeff. ($T_m(\lambda_{ieff})$)** |
| 1 | 0.669 | 0.625621 | 0.625247 | 0.635784 | 0.642749 | 0.626039 | 0.7995 |
| 2 | 0.685 | 0.649187 | 0.648802 | 0.659662 | 0.66684 | 0.649618 | 0.824 |
| 3 | 0.693 | 0.714684 | 0.714261 | 0.724964 | 0.73398 | 0.715157 | 0.904077 |
| 4 | 0.698 | 0.743767 | 0.743617 | 0.754764 | 0.76295 | 0.744449 | 0.939667 |
| 5 | 0.741 | 0.764682 | 0.761883 | 0.775452 | 0.781246 | 0.771053 | 0.9488 |
| 6 | 0.753 | 0.795327 | 0.78151 | 0.79389 | 0.811922 | 0.804646 | 0.96961 |

**Table A-4**

| Total spectral optical depth for a slant path of the atmosphere ($\tau_{atm}(\lambda_{i\,eff})$) | | | | | | | |
|---|---|---|---|---|---|---|---|
| $i$ | $\lambda_{i\,eff}(\mu m)$ | **May21, 2008; 5.24(LT), $m(\theta)$=1.167** | **May21, 2008; 6.10(LT), $m(\theta)$=1.005** | **May21, 2008; 7.00(LT), $m(\theta)$=1.015** | **May21, 2008; 8.00(LT), $m(\theta)$=1.305** | **May23, 2008; 5.25(LT), $m(\theta)$=1.167** | **Molecular optical depth ($\tau_M$)** |
| 1 | 0.669 | 0.469011 | 0.469609 | 0.452896 | 0.442001 | 0.468343 | 0.223769 |
| 2 | 0.685 | 0.432035 | 0.432628 | 0.416028 | 0.405205 | 0.431371 | 0.193585 |
| 3 | 0.693 | 0.335915 | 0.336506 | 0.321633 | 0.309273 | 0.335254 | 0.100841 |
| 4 | 0.698 | 0.296027 | 0.29623 | 0.281351 | 0.270563 | 0.295111 | 0.06223 |
| 5 | 0.741 | 0.268296 | 0.271962 | 0.25431 | 0.246866 | 0.259998 | 0.052557 |
| 6 | 0.753 | 0.229002 | 0.246527 | 0.23081 | 0.208351 | 0.217353 | 0.030861 |

Then using Eq. (4.3.4), aerosol optical thickness (AOT= $\tau_A(\lambda_{ieff})$), for a slant path of the atmosphere can be determined (given below).

**Table A-5**

| **Aerosol optical depth (AOD) ( $\tau_A(\lambda_{ieff}) = [\ln V_0(\lambda_{ieff}) - \ln(\gamma^2 V(\lambda_{ieff})) - \tau_M]$)** | | | | | | |
|---|---|---|---|---|---|---|
| $i$ | $\lambda_{ieff}(\mu m)$ | **May21, 2008; 5.24(LT), $m(\theta)$=1.167** | **May21, 2008; 6.10(LT), $m(\theta)$=1.005** | **May21, 2008; 7.00(LT), $m(\theta)$=1.015** | **May21, 2008; 8.00(LT), $m(\theta)$=1.305** | **May23, 2008; 5.25(LT), $m(\theta)$=1.167** |
| 1 | 0.669 | 0.245243 | 0.24584 | 0.229127 | 0.218232 | 0.244574 |
| 2 | 0.685 | 0.23845 | 0.239043 | 0.222443 | 0.21162 | 0.237786 |
| 3 | 0.693 | 0.235074 | 0.235666 | 0.220792 | 0.208432 | 0.234413 |
| 4 | 0.698 | 0.233798 | 0.234 | 0.219121 | 0.208333 | 0.232881 |
| 5 | 0.741 | 0.215738 | 0.219405 | 0.201752 | 0.194309 | 0.207441 |
| 6 | 0.753 | 0.198141 | 0.215666 | 0.199949 | 0.17749 | 0.186492 |

Thus measurements of aerosol optical thickness at more than one wavelength used for retrieving the aerosol size distribution and the complex refractive index.

# Bibliography

[1] Salby, M.L. (1996). Fundamentals of Atmospheric Physics. Academic Press, San Diego.

[2] Malm W., J. Sisler, D. Huffman, R. Eldred, and T. Cahill, 1994: Spatial and seasonal trends in particle concentration and optical extinction in the United States. J. Geophys. Res. 99:1347-1370.

[3] Mishchenko M., et al., 2007a: Accurate monitoring of terrestrial aerosols and total solar irradiance. Bull. Amer. Meteorol. Soc. 88:677-691.

[4] Andreae, M. O. and Crutzen, P. J. [1997]. Atmospheric aerosols: Biogeochemical sources and role in atmospheric chemistry. Science 276(5315), 1052–1058.

[5] Charlson, R. J., Schwartz, S. E., Hales, J. M., Cess, R. D., Coakley, J. A., Hansen, J. E. and Hofmann, D. J. [1992]. Climate forcing by anthropogenic aerosols. Science 255(5043), 423–430.

[6] D'Almeida, G. A., P. Koepke, and E. P. Shettle. Atmospheric Aerosol Global Climatology and Radiative Characteristics, Deepak Publ., 1991.

[7] Roedel, W., Physik unserer Umwelt. Atmospheric Aerosol, Springer Verlag, Berlin, 1992.

[8] Heintzenberg, J., C. D. Covert, and R. van Dingen. Size distribution and chemical composition of marine aerosols: a compilation and review, Tellus-Series B, Chem. Phys. Met., 52B(4), 1104–1122, 2000.

[9] Husar, R. B., J. M. Prospero, and L. L. Stowe. Characterization of tropospheric aerosol over the ocean with the NOAA Advanced Very High Resolution Radiometer optical thickness operational product, J. Geophys. Res., 102, 16889–16909, 1997.

[10] Song-Miao, F., L. W. Horowitz, H. L. II, and W. J. Moxim. Impact of air pollution on wet deposition of mineral dust aerosols, Geophys. Res. Lett., 31, doi: 10.1029/2003GL018501, L02104, 1–4, 2004.

[11] Maring, H., D. L. Savoie, M. A. Izaguirre, L. Custals, and J. S. Reid. Mineral dust aerosol size distribution change during atmospheric transport, J. Geophys. Res., 108, doi: 10.1029/2002JD002536, PRD8 1–6, 2003.

[12] Geogdzhayev, I. V., M. I. Mishchenko, L. Liu , and L. Remer. Global two-channel AVHRR aerosol climatology: effects of stratospheric aerosols and preliminary comparisons with MODIS and MISR retrievals, J. Quant. Spectrosc. Radiat. Transfer, 88, 1-3, 2004.

[13] Haywood, J. M., and O. Boucher. Estimates of the direct and indirect radiative forcing due to tropospheric aerosols: a review, Reviews of Geophysics, 38(4), 513–543, 2000.

[14] Twomey, S., The Influence of Pollution on the short-wave albedo of clouds, J. Atmos. Sci., 34 , 1149–1152, 1977.

[15] Ghan S. J., and S.E. Schwartz, 2007. Aerosol Properties and Processes: A Path from Field and Laboratory Measurements to Global Climate Models. Bull. Amer. Meteorol. Soc. 88, 1059–1083.

[16] Berresheim, H., Wine, P.H. & Davis, D.D. (1995). Sulfur in the atmosphere. In Singh, H.B. (ed.). Composition, Chemistry and Climate of the Atmosphere. Van Nostrand Reinhold, New York.

[17] Finlayson-Pitts, B. & Pitts, J. (1999). Chemistry of the Upper and Lower Atmosphere. Acadamic Press, New York.

[18] Pueschel, R.F. (1995). Atmospheric aerosols. In Singh, H.B. (ed.). Composition, Chemistry and Climate of the Atmosphere. Van Nostrand Reinhold, New York.

[19] Jaenicke, R. (1988). Atmospheric physics and chemistry. In Fischer, G. (ed.). Meteorology: Physical and Chemical Properties of Air. Springer-Verlag, Berlin.

[20] Y. J. Kaufman et al., 1997. Passive remote sensing of troposhpeic aerosol and atmospheric correction for the aerosol effect, J. G., VOL. 102, NO. D14, 16815-16830.

[21] Jacson,David.John.(1999). Clasical Electrodynamics,3rd edition, printed in the united states of America

[22] Liuo, Nan, Kuo. (1983). An Introduction to Atmospheric physics, Acadamic press,inc.

[23] Iogra,Gabriela and Stefan,Sabina.(2005). Effects of the atmospheric aerosol on the optical properties of cloud,Romanian reports in physics,Vol.57,No.3,P.426- 435.

[24] Arfken, G., Mathematical Methods for Physicists, third ed., Academic Press, San Diego, CA, 1985.

[25] Bohren,C.F and Huffman,D.R.(1983). Absorption and scattering of light by small particles.New York:Wiley.

[26] Abramowitz, M., and I. Stegun, Handbook of Mathematical Functions, Dover, New York, 1964.

[27] Iqbal, M. (1983). An Introduction to Solar Radiation. Academic Press, Toronto.

[28] De More, W.B., Sander, S.P., Golden, D.M. et al. (1997). Chemical Kinetics and Photochemical Data for Use in Stratospheric Modeling. Evaluation No. 12. Jet

[29] Coulson, K.L. Solar and terrestrial radiation. Academic Press, 1975.

[30] Young A T 1981. On the Rayleigh scattering optical depth of atmosphere; *J. Appl. Meteorol.* 20 328.

[31] King M D, Byrne D M, Herman B M and Reagan J A 1978. Aerosol size distributions obtained by inversion of spectral optical depth measurements; *J. Atmos. Sci.* 35 2153.

[32] King M D 1982 Sensitivity of constrained linear inversion to the selection of Lagrange multiplier; *J. Atmos. Sci.* 39 1356.

[33] Dubovik, O., Holben,N.B.,Lapyonok,T., and et al.,.(2002). Non-spherical aerosol retrieval method employing light scattering by spheroids, geophysical research letters,vol.29,no.10,10.1029/2001glo,145-606.

[34] Hand, I. F., 1946: Pyrheliometers and Pyrheliometric Measurements, U.S. Weather Bureau

[35] Holben,B.N., et al.,.(1998). AERONET-A fedrated instrument network and data archive for aerosol characterization, Remote sens,Environ,66,1-16,1998.

[36] Kay, M. J. and Box, M. A. 2000. Radiative effects of absorbing aerosols and the impact of water vapour. J. Geophys. Res., 105, 12,221-12,234.

[37] D'Almeda, G. A., Koepke, P., and Shettle, E. P. 1991. Atmospheric Aerosols: Global Climatology and Radiative Characteristics. A. Deepak Publishing, 561 pp.

[38] Swietlicki, E., J. Zhou, O.H. Berg, B.G. Martinsson, G.Frank, S.-I. Cederfelt, U. Dusek, A. Berner, W. Birmili, A. Wiedensohler, B. Yuskiewicz, and K.N. Bower, 1999. A closure study of sub-micrometer aerosol particle hygroscopic behaviour. *Atmos. Res*., 205-240.

[39] D'Almeida, G. A.: On the variability of desert aerosol radiative characteristics, J. Geophys. Res., 92, 3017–3026, 1987.

[40] Sokolik, I. N., Andronova, A., and Johnson, T. C.: Complex refractive index of atmospheric dust aerosols, Atmos. Environ., 27, 2495–2502, 1993.